YITP-SB-99-65

$\overline{\rm MS}$ Parton densities with NNLO heavy flavor matching conditions

A. Chuvakin, J. Smith
C.N. Yang Institute for Theoretical Physics,
State University of New York at Stony Brook, New York 11794-3840.

November 1999

Abstract

A study is made of charm and bottom flavor matching conditions on parton densities. Starting from an $\overline{\rm MS}$ three-flavor density set, where the scale $\mu < m_c$, and using the recently derived two-loop matching conditions, we provide a new set of four-flavor parton densities where $m_c \leq \mu < m_b$ and five-flavor densities where $\mu \geq m_b$. The effect of the next-to-next-to-leading order matching conditions on the evolution equations is important for scales just above the transition regions. This includes the small x and small Q^2 domain studied by the H1 and ZEUS experiments at HERA. At small x the effects of the matching conditions never die away even for large μ^2.

PACS numbers: 11.10Jj, 12.38Bx, 13.60Hb, 13.87Ce.

1 Introduction

Quantum chromodynamic predictions for experimental cross sections and distributions in perturbation theory rely heavily on accurate knowledge of parton densities. Several groups [1], [2], [3] have extracted these densities from global fits to data with the latest theoretical information on $\overline{\rm MS}$ coefficient functions. At present the evolution of these densities via the Altarelli-Parisi (AP) equations [4] uses the information on leading order (LO) and next-to-leading order (NLO) [5] splitting functions. Unfortunately the next-to-next-to-leading order (NNLO) splitting functions are not known but some interesting pieces of information are available [6], [7], [8]. The complete splitting functions should be known soon.

The description of heavy quarks within this analysis recently received a lot of attention due to the data on deep inelastic production of D^* mesons from HERA [9], [10]. The global fitting groups have adopted different approaches. The CTEQ5 analysis describes charm and bottom densities via the so-called ACOT prescription [11], which is a one-loop matching condition between three-flavor and four-flavor densities at the scale $\mu = m_c$ and a corresponding one-loop matching between the four-flavor and five-flavor densities at the scale $\mu = m_b$. This is not done in the MRST density sets. Instead they impose matching conditions that the logarithmic derivative of the deep inelastic structure functions with regard to the scale μ should be continuous, see [12] for details. This yields different charm and bottom densities. The GRV group [13] adopt the approach that one does not need any densities other than a three-flavor $\overline{\rm MS}$ set because the convolution of these densities with the NLO heavy quark coefficient functions provided in [14] yields an excellent fit to the presently available data on $F_{2,c}(x, Q^2, m_c^2)$, which is stable under scale variations. By never taking the limit that $m_c \to 0$ the theoretical prediction has no collinear singularity problem. Note that the physical threshold for a heavy quark antiquark pair is at $Q^2(1-x)/x = 4m^2$. However the physical threshold is distinct from the matching scale where one switches between parton density sets.

The parton densities with n_f and $n_f + 1$ flavors are related by a set of operator matrix elements (OME's). The order α_s^2 OME's were recently derived in [15]. They contain terms with $\ln^i(\mu^2/m^2)$ $i = 1, 2$ as well as non-logarithmic terms. They have the property that the $n_f + 1$ flavor densities vanish in LO and in NLO when the scale $\mu = m$. In NNLO there are finite x-

dependent discontinuities at this scale, which we refer to as NNLO matching conditions. In this respect the matching conditions on the parton densities are similar to those for the two-loop running coupling constant derived in [19], [20]. These NNLO matching conditions can be important numerically. Note that the running coupling constant is not small at the scale $\mu = m_c$. The charm density constructed from the two-loop matching conditions has been used in a recent study of variable flavor number schemes for the charm component of the deep inelastic structure functions [16]. Here we would like to present a complete set of parton densities for light (u,d,s,g) and heavy (c,b) partons which satisfy the NNLO boundary conditions and are evolved with NLO splitting functions. When the three-loop anomalous dimensions become available they can be included in this analysis. At present our study primarily focuses on the effects of the discontinuous matching conditions and the differences between the resulting three, four and five-flavor parton densities as the scale μ increases through the regions $m_c \leq \mu < m_b$ and $\mu \geq m_b$ respectively.

In Sec. II we present some technical details about our choice of input parton densities and the two-loop matching conditions. All densities are derived in the $\overline{\rm MS}$ scheme. Then in Sec.III we give plots of the parton densities. Finally comparisons are made between the presently available NLO sets and our (NNLO) set. A discussion of the solutions of the evolution equations is given in the Appendix. We intend to make our computer package for these densities available in due course.

2 The parton densities

We present a consistent set of $\overline{\rm MS}$ parton densities containing three, four and five flavors for scales satisfying $\mu < m_c$, $m_c \leq \mu < m_b$ and $\mu \geq m_b$ respectively. The evolution of the densities is done with our own computer code written in C++ and some details are given in the Appendix. The code uses the direct x-space method to solve the evolution equation [4] similar to that in [17] and allows us to evolve both light and heavy parton densities in LO, NLO and NNLO (the latter using the NLO weights). The weights for the calculation are computed analytically from the LO and NLO [5] $\overline{\rm MS}$ splitting functions thus removing possible instabilities in the numerical integrations. Hence the program is very efficient and fast. The results from the evolution code have been thoroughly checked against the tables in the HERA report [18]. We use weights in LO and NLO for $n_f = 3, 4, 5$ for evolving the gluon $f_g^{\rm S}(n_f, x, \mu^2)$, the singlet quark densities $f_q^{\rm S}(n_f, x, \mu^2)$, the non-singlet valence quark densities $f_{k-\bar{k}}(n_f, x, \mu^2)$ and the non-singlet sea quark densities $f_q^{\rm NS}(n_f, x, \mu^2)$. As the scale increases across the charm and bottom matching points the sets are redefined to include densities for the c and b heavy quarks. The program allows us to use LO, NLO or NNLO matching conditions for the generation of the heavy flavor densities.

The number densities are defined as

$$\begin{aligned} f_{k-\bar{k}}(n_f, x, \mu^2) &\equiv f_k(n_f, x, \mu^2) - f_{\bar{k}}(n_f, x, \mu^2)\,,\ k = u, d \\ f_{k+\bar{k}}(n_f, x, \mu^2) &\equiv f_k(n_f, x, \mu^2) + f_{\bar{k}}(n_f, x, \mu^2)\,,\ k = u, d, s, c, b \end{aligned} \tag{2.1}$$

$$f_q^{\rm S}(n_f, x, \mu^2) = \sum_{k=1}^{n_f} f_{k+\bar{k}}(n_f, x, \mu^2) \tag{2.2}$$

$$f_q^{\rm NS}(n_f, x, \mu^2) = f_{k+\bar{k}}(n_f, x, \mu^2) - \frac{1}{n_f} f_q^{\rm S}(n_f, x, \mu^2)\,. \tag{2.3}$$

We start our LO evolution using the following input from [2] at $\mu_0^2 = \mu_{\rm LO}^2 = 0.26$ (GeV/c^2)^2

$$\begin{aligned} x f_{u-\bar{u}}(3, x, \mu_0^2) &= x u_v(x, \mu_{\rm LO}^2) \\ &= 1.239\ x^{0.48}\,(1-x)^{2.72}\,(1 - 1.8\sqrt{x} + 9.5x) \end{aligned}$$

$$
\begin{aligned}
x f_{d-\bar{d}}(3,x,\mu_0^2) &= x d_v(x,\mu^2_{\rm LO}) \\
&= 0.614\ (1-x)^{0.9}\ x u_v(x,\mu^2_{\rm LO}) \\
x(f_{\bar{d}}(3,x,\mu_0^2) - f_{\bar{u}}(3,x,\mu_0^2)) &= x\Delta(x,\mu^2_{\rm LO}) \\
&= 0.23\ x^{0.48}\,(1-x)^{11.3}\,(1-12.0\sqrt{x}+50.9x) \\
x(f_{\bar{d}}(3,x,\mu_0^2) + f_{\bar{u}}(3,x,\mu_0^2)) &= x(\bar{u}+\bar{d})(x,\mu^2_{\rm LO}) \\
&= 1.52\ x^{0.15}\,(1-x)^{9.1}\,(1-3.6\sqrt{x}+7.8x) \\
x f_g(3,x,\mu_0^2) &= x g(x,\mu^2_{\rm LO}) \\
&= 17.47\ x^{1.6}\,(1-x)^{3.8} \\
x f_s(3,x,\mu_0^2) = x f_{\bar{s}}(3,x,\mu_0^2) &= x s(x,\mu^2_{\rm LO}) \\
&= x\bar{s}(x,\mu^2_{\rm LO}) = 0\,. \qquad (2.4)
\end{aligned}
$$

Here $\Delta \equiv \bar{d} - \bar{u}$ is used to construct the non-singlet combination. We start the corresponding NLO evolution using the following input from [2] at $\mu_0^2 = \mu^2_{\rm NLO} = 0.40\ ({\rm GeV/c^2})^2$

$$
\begin{aligned}
x f_{u-\bar{u}}(3,x,\mu_0^2) &= x u_v(x,\mu^2_{\rm NLO}) \\
&= 0.632\ x^{0.43}\,(1-x)^{3.09}\,(1+18.2x) \\
x f_{d-\bar{d}}(3,x,\mu_0^2) &= x d_v(x,\mu^2_{\rm NLO}) \\
&= 0.624\ (1-x)^{1.0}\ x u_v(x,\mu^2_{\rm NLO}) \\
x(f_{\bar{d}}(3,x,\mu_0^2) - f_{\bar{u}}(3,x,\mu_0^2)) &= x\Delta(x,\mu^2_{\rm NLO}) \\
&= 0.20\ x^{0.43}\,(1-x)^{12.4}\,(1-13.3\sqrt{x}+60.0x) \\
x(f_{\bar{d}}(3,x,\mu_0^2) + f_{\bar{u}}(3,x,\mu_0^2)) &= x(\bar{u}+\bar{d})(x,\mu^2_{\rm NLO}) \\
&= 1.24\ x^{0.20}\,(1-x)^{8.5}\,(1-2.3\sqrt{x}+5.7x) \\
x f_g(3,x,\mu_0^2) &= x g(x,\mu^2_{\rm NLO}) \\
&= 20.80\ x^{1.6}\,(1-x)^{4.1} \\
x f_s(3,x,\mu_0^2) = x f_{\bar{s}}(3,x,\mu_0^2) &= x s(x,\mu^2_{\rm NLO}) \\
&= x\bar{s}(x,\mu^2_{\rm NLO}) = 0. \qquad (2.5)
\end{aligned}
$$

From the above densities we form the combinations that we evolve and step across thresholds. The NNLO densities for $\mu^2_{\rm NLO} < \mu^2 < m_{\rm c}^2$ are replaced with NLO densities. The heavy quark masses $m_c = 1.4\ {\rm GeV/c^2}$, $m_b = 4.5\ {\rm GeV/c^2}$ are used throughout the calculation together with the exact expression for the running coupling constant $\alpha_s(\mu^2)$, represented as the solution of the following

differential equation

$$\frac{d\,\alpha_s(\mu^2)}{d\,\ln(\mu^2)} = -\frac{\beta_0}{4\pi}\,\alpha_s^2(\mu^2) \;-\; \frac{\beta_1}{16\pi^2}\,\alpha_s^3(\mu^2) \tag{2.6}$$

or in the implicit form

$$\ln\frac{\mu^2}{(\tilde{\Lambda}^{(n_f)}_{\rm EXACT})^2} = \frac{4\pi}{\beta_0\alpha_s(\mu^2)} \;-\; \frac{\beta_1}{\beta_0^2}\,\ln\left[\frac{4\pi}{\beta_0\alpha_s(\mu^2)} \;+\; \frac{\beta_1}{\beta_0^2}\right], \tag{2.7}$$

where $\beta_0 = 11 - 2n_f/3$ and $\beta_1 = 102 - 38n_f/3$. The values for $\tilde{\Lambda}^{(n_f)}_{\rm EXACT}$ are carefully chosen to obtain accurate matching at the scales m_c^2 and m_b^2 respectively. We used the values $\tilde{\Lambda}^{(3,4,5,6)}_{\rm EXACT} = 299.4,\ 246,\ 167.7,\ 67.8\ {\rm MeV}/c^2$ respectively in the exact formula (which yields $\alpha_s^{\rm EXACT}(m_Z^2) = 0.114$, $\alpha_s^{\rm EXACT}(m_b^2) = 0.205$, $\alpha_s^{\rm EXACT}(m_c^2) = 0.319$, $\alpha_s^{\rm EXACT}(\mu^2_{\rm NLO}) = 0.578$) and $\Lambda^{(3,4,5,6)}_{\rm LO} = 204,\ 175,\ 132, 66.5\ {\rm MeV}/c^2$ respectively (which yields $\alpha_s^{\rm LO}(m_Z^2) = 0.125$, $\alpha_s^{\rm LO}(m_b^2) = 0.232$, $\alpha_s^{\rm LO}(m_c^2) = 0.362$, $\alpha_s^{\rm LO}(\mu^2_{\rm LO}) = 0.763$) for the LO formula. Note that we have not used the two-loop matching of the running coupling constant $\alpha_s(\mu^2)$ at the same scales from [19],[20] to focus on the matching conditions on the flavor densities. Numerically the discontinuity in the running coupling constant across the charm threshold is aproximately two parts in one thousand, which is far too small to affect our results.

Three flavor evolution proceeds from the initial μ_0^2 to the scale $\mu^2 = m_c^2 = 1.96\ ({\rm GeV/c^2})^2$. At this point the charm density is then defined by

$$\begin{aligned} f_{c+\bar{c}}(n_f+1, m_c^2) \;&=\; a_s^2(n_f, m_c^2)\Big[\tilde{A}^{\rm PS}_{Qq}(1) \otimes f_q^{\rm S}(n_f, m_c^2) \\ &\quad + \tilde{A}^{\rm S}_{Qg}(1) \otimes f_g^{\rm S}(n_f, m_c^2)\Big], \end{aligned} \tag{2.8}$$

with $n_f = 3$ and $a_s = \alpha_s/4\pi$. We have suppressed the x dependence to make the notation more compact. The $\otimes$ symbol denotes the convolution integral $f \otimes g = \int f(x/y)g(y)dy/y$, where $x \le y \le 1$ The OME's $\tilde{A}^{\rm PS}_{Qq}(\mu^2/m_c^2)$, $\tilde{A}^{\rm S}_{Qg}(\mu^2/m_c^2)$ are given in [15]. The reason for choosing the matching scale μ at the mass of the charm quark m_c is that all the $\ln(\mu^2/m_c^2)$ terms in the OME's vanish at this point leaving only the nonlogarithmic pieces in the order α_s^2 OME's to contribute to the right-hand-side of Eq.(2.8). Hence the LO and NLO charm densities vanish at the scale $\mu = m_c$. The NNLO charm

density starts off with a finite x-dependent shape in order a_s^2. Note that we then order the terms on the right-hand-side of Eq.(2.8) so that the result contains a product of NLO OME's and LO parton densities. The result is then of order a_s^2 and should be multiplied by order a_s^0 coefficient functions when forming the deep inelastic structure functions.

The four-flavor gluon density is also generated at the matching point in the same way. At $\mu = m_c$ we define

$$\begin{aligned} f_g^{\rm S}(n_f+1,m_c^2) &= f_g^{\rm S}(n_f,m_c^2) \\ &\quad + a_s^2(n_f,m_c^2)\Big[A_{gq,Q}^{\rm S}(1)\otimes f_q^{\rm S}(n_f,m_c^2)\,, \\ &\quad + A_{gg,Q}^{\rm S}(1)\otimes f_g^{\rm S}(n_f,m_c^2)\Big]\,. \end{aligned} \tag{2.9}$$

The OME's $A_{gq,Q}^{\rm S}(\mu^2/m_c^2)$, $A_{gg,Q}^{\rm S}(\mu^2/m_c^2)$ are given in [15]. The four-flavor light quark (u,d,s) densities are generated using

$$\begin{aligned} f_{k+\bar{k}}(n_f+1,m_c^2) &= f_{k+\bar{k}}(n_f,m_c^2) \\ &\quad + a_s^2(n_f,m_c^2)A_{qq,Q}^{\rm NS}(1)\otimes f_{k+\bar{k}}(n_f,m_c^2)\,. \end{aligned} \tag{2.10}$$

The OME $A_{qq,Q}^{\rm NS}(\mu^2/m_c^2)$ is given in [15] and the *total* four-flavor singlet quark density in Eq.(2.2) follows from the sum of Eqs.(2.8) and (2.10). The non-singlet density then follows from Eq.(2.1). In Eqs.(2.9) and (2.10) $n_f = 3$. The remarks after Eq.(2.8) are relevant here too.

Next the resulting four-flavor densities are evolved using the four-flavor weights in either LO or NLO up to the scale $\mu^2 = 20.25$ $(\mathrm{GeV/c^2})^2$. The bottom quark density is then generated at this point using

$$\begin{aligned} f_{b+\bar{b}}(n_f+1,m_b^2) &= a_s^2(n_f,m_b^2)\Big[\tilde{A}_{Qq}^{\rm PS}(1)\otimes f_q^{\rm S}(n_f,m_b^2) \\ &\quad + \tilde{A}_{Qg}^{(\rm S)}(1)\otimes f_g^{\rm S}(n_f,m_b^2)\Big]\,, \end{aligned} \tag{2.11}$$

and the gluon and light quark densities (which now include charm) are generated using Eqs.(2.8)-(2.10) with $n_f = 4$ and replacing m_c^2 by m_b^2. Therefore only the nonlogarithmic terms in the order a_s^2 OME's contribute to the matching conditions on the bottom quark density. Then all the densities are evolved up to higher μ^2 as a five-flavor set with either LO or NLO splitting functions. This is valid until $\mu = m_t \approx 175$ $\mathrm{GeV/c^2}$ above which one should switch to a six-flavor set. We do not implement this step because the top quark density would be extremely small.

The procedure outlined above generates a full set of parton densities (gluon, singlet, non-singlet light and heavy quark densities,) for any x and μ^2 from the three-flavor LO and NLO inputs in Eqs.(2.4) and (2.5). Note that one could also use the formulae above in fixed order perturbation theory. In this case the four-flavour densities are defined by extending the integrals on the right-hand sides of Eqs.(2.8)-(2.11) to

$$\begin{aligned} f_{c+\bar{c}}(n_f+1,\mu^2) &= a_s(n_f,\mu^2)\tilde{A}^{\rm S}_{Qg}\Big(\frac{\mu^2}{m_c^2}\Big)\otimes f_g^{\rm S}(n_f,\mu^2) \\ &\quad +a_s^2(n_f,\mu^2)\Big[\tilde{A}^{\rm PS}_{Qq}\Big(\frac{\mu^2}{m_c^2}\Big)\otimes f_q^{\rm S}(n_f,\mu^2) \\ &\quad +\tilde{A}^{\rm S}_{Qg}\Big(\frac{\mu^2}{m_c^2}\Big)\otimes f_g^{\rm S}(n_f,\mu^2)\Big]\,, \end{aligned} \tag{2.12}$$

$$\begin{aligned} f_g^{\rm S}(n_f+1,\mu^2) &= f_g^{\rm S}(n_f,\mu^2) \\ &\quad +a_s(n_f,\mu^2)A^{\rm S}_{gg,Q}(\frac{\mu^2}{m_c^2})\otimes f_g^{\rm S}(n_f,\mu^2) \\ &\quad +a_s^2(n_f,\mu^2)\Big[A^{\rm S}_{gq,Q}(\frac{\mu^2}{m_c^2})\otimes f_q^{\rm S}(n_f,\mu^2)\,, \\ &\quad +A^{\rm S}_{gg,Q}(\frac{\mu^2}{m_c^2})\otimes f_g^{\rm S}(n_f,\mu^2)\Big]\,, \end{aligned} \tag{2.13}$$

and

$$\begin{aligned} f_{k+\bar{k}}(n_f+1,\mu^2) &= f_{k+\bar{k}}(n_f,\mu^2) \\ &\quad +a_s^2(n_f,\mu^2)A^{\rm NS}_{qq,Q}\Big(\frac{\mu^2}{m_c^2}\Big)\otimes f_{k+\bar{k}}(n_f,\mu^2)\,, \end{aligned} \tag{2.14}$$

for $n_f = 3$ and $m_c^2 \leq \mu^2 < m_b^2$. Then the five-flavor densities are defined by

$$\begin{aligned} f_{b+\bar{b}}(n_f+1,\mu^2) &= a_s(n_f,\mu^2)\tilde{A}^{\rm S}_{Qg}\Big(\frac{\mu^2}{m_b^2}\Big)\otimes f_g^{\rm S}(n_f,\mu^2) \\ &\quad +a_s^2(n_f,\mu^2)\Big[\tilde{A}^{\rm PS}_{Qq}\Big(\frac{\mu^2}{m_b^2}\Big)\otimes f_q^{\rm S}(n_f,\mu^2) \end{aligned}$$

$$+\tilde{A}_{Qg}^{\rm S)}\Big(\frac{\mu^2}{m_b^2}\Big)\otimes f_g^{\rm S}(n_f,\mu^2)\Big]\,, \tag{2.15}$$

for $n_f = 4$ and $\mu^2 \geq m_b^2$. Also one should replace $n_f = 4$ and m_c^2 by m_b^2 in Eqs.(2.12)-(2.14). In this case no four-flavor or five-flavour evolution is made so the logarithmic terms in μ^2/m_c^2 and/or μ^2/m_b^2 are not summed. We will show the differences between this fixed order perturbation theory (FOPT) treatment and the evolved treatment in the next Section.

3 Results

Here we present results from the evolution of the parton densities. The inputs are the three-flavor densities at μ_0 in Eqs.(2.4),(2.5) which are evolved up to the scale $\mu = m_c = 1.4$ GeV/c^2. During this evolution the number of light flavors $n_f = 3$ in both the $\overline{\rm MS}$ splitting functions and the running coupling constant.

We start by giving the four-flavor densities, where $n_f = 4$, in the region between $m_c \leq \mu < m_b$ which follow by evolution from the matching conditions in Eqs. (2.8)-(2.10). We present results at the scales $\mu^2 = 1.96$, 2, 3, 4, 5, 10 and 20 in units of (GeV/c^2)^2. First we show the charm density $xc^{\rm NNLO}(4, x, \mu^2)$ in two ranges (a) $10^{-5} < x < 1$ and (b) $10^{-2} < x < 1$ in Figs.1(a) and 1(b) respectively. We notice that this density starts off negative at small x but it is positive at large x so that the momentum sum rule is satisfied. To show the effect of resumming the logarithmic terms via the evolution equation from the charm threshold as compared with just computing the integrals in Eq. (2.12) at all scales μ we show in Fig.1(c) the ratios $R_c^{\rm NNLO}(x, \mu^2) = xc_{\rm EVOLVED}(4, x, \mu^2)/xc_{\rm FOPT}(4, x, \mu^2)$. Here FOPT stands for fixed order perturbation theory. The effects of the evolution are especially significant at small x and large x. Notice that the discontinuity at $x \approx 0.01$ is caused by the change in sign of the NNLO charm quark density. For a comparison we have also shown the NLO results from the MRST98 set 1 [3] and CTEQ5HQ [1] parton density sets in Figs. 1(d) and (e). These groups use different input densities so a direct comparison does not have any true significance. Nevertheless our density is larger than the MRST98 set 1 result and smaller than the CTEQ5HQ result at small x and large μ^2.

In Fig.2(a) we show the four-flavor gluon density $xg^{\rm NNLO}(4, x, \mu^2)$ in the same range $10^{-5} < x < 1$ for the same scales as in Fig.1. We also show in Fig.2(b) the ratios $R_g^{\rm NNLO}(x, \mu^2) = xg_{\rm EVOLVED}(4, x, \mu^2)/xg_{\rm FOPT}(4, x, \mu^2)$ for the same scales, where we use Eq.(2.13) for the FOPT density. The effect of the suppression of the charm density at small x translates into an increase of the gluon density at small x. For comparison we show the three-flavor NLO gluon density in Fig. 2(c). We have also shown the NLO results from the MRST98 set 1 and CTEQ5HQ parton density sets in Figs. 2(d) and (e). These densities do not increase as rapidly at large μ^2 because they use different inputs.

In Fig.3(a) we show the singlet quark density $x\Sigma^{\rm NNLO}(4, x, \mu^2)$ in the

range $10^{-5} < x < 1$ for the same scales as above. Then is Fig.3(b) we show the ratios $R_\Sigma^{\rm NNLO}(x,\mu^2) = x\Sigma_{\rm EVOLVED}(4,x,\mu^2)\ /x\Sigma_{\rm FOPT}(4,x,\mu^2)$, where we use Eq.(2.14) for the FOPT density. This ratio shows increases or decreases depending on the x and μ^2 values. It is appreciably smaller at large μ^2, which reflects the differences between the three-flavor and four-flavor gluon densities. For comparison we show the three-flavor NLO density in Fig.3(c).

Next in Fig.4(a) we show the nonsinglet density $x\sigma^{\rm NNLO}(4,x,\mu^2)$, where $\sigma = (u+\bar{u})/2$, in the range $10^{-5} < x < 1$ for the same scales. In Fig.4(b) we show the ratios $R_\sigma^{\rm NNLO}(x,\mu^2) = x\sigma_{\rm EVOLVED}(4,x,\mu^2)/x\sigma_{\rm FOPT}(4,x,\mu^2)$ for the same scales, where we use Eq.(2.14) for the FOPT density. The ratio is significantly below unity at large x. In Fig.4(c) we show the three-flavor NLO result. The difference is small.

We complete our presentation of four-flavor densities by showing in Fig.5(a) the strange quark density $xs^{\rm NNLO}(4,x,\mu^2)$ in the range $10^{-5} < x < 1$. In Fig.5(b) we show the ratios $R_g^{\rm NNLO}(x,\mu^2) = xs^{\rm EVOLVED}(4,x,\mu^2)/xs^{\rm FOPT}(4,x,\mu^2)$ for the same scales. In Fig.5(c) we show the three-flavor NLO density, where again the difference is small. We have checked that these densities satisfy the momentum sum rule for four flavors.

Now we move up in scale to consider $\mu > m_b = 4.5$ GeV/c^2 which is the five-flavor region. The parton densities in this region are now generated from the previous four-flavor set by using the conditions in the Eqs.(2.8) -(2.10) with $n_f = 4$ at $\mu^2 = m_b^2$ and replacing m_c^2 by m_b^2. Here we show plots for the scales μ^2 =20.25, 25, 30, 40, and 100 in units of (GeV/c^2)^2.

The first density to consider is the bottom quark density. We show in Fig.6(a) $xb^{\rm NNLO}(5,x,\mu^2)$ in the range $10^{-5} < x < 1$ for the scales mentioned above. Notice that it is negative for small x and small μ^2, The region $10^{-2} < x < 1$ is shown in Fig. 6(b) to demonstrate that the density is positive for large x. In this respect it is like the charm density in the region just above the four-flavor matching point. In Fig.6(c) we show the ratios $R_g^{\rm NNLO}(x,\mu^2) = xb^{\rm EVOLVED}(5,x,\mu^2)/xb^{\rm FOPT}(5,x,\mu^2)$, where Eq.(2.15) is used for the FOPT density. Here it is clear that the effect of the evolution is appreciable at small x. For a comparison we have also shown the NLO results from the MRST98 set 1 and CTEQ5HQ parton density sets in Figs. 1(d) and (e). Note that these groups use different input densities so a direct comparison does not have any true significance. Nevertheless both bottom densities are larger than ours at small x and large μ^2.

The five-flavor charm density $xc^{\rm NNLO}(5,x,\mu^2)$ is shown in Fig.7(a) in the

range $10^{-5} < x < 1$ for the same scales. In this case the ratios of the evolved densities to the FOPT densities is very close to unity for all x and μ^2 values so we do not show a plot. For a comparison we have also shown the NLO results from the MRST98 set 1 and CTEQ5HQ parton density sets in Figs. 1(b) and (c). The former has a smaller density at large μ^2 and the latter a larger density.

Next we show in Fig.8(a) the gluon density $xg^{\rm NNLO}(5, x, \mu^2)$ in the range $10^{-5} < x < 1$ for the same scales. In this case the ratios of the evolved densities to the FOPT densities is very close to unity for all x and μ^2 values so we do not show a plot. In Fig.8(b) we show the corresponding three-flavor NLO density. The latter is larger at small x and large μ^2.

In Fig.9(a) we show the nonsinglet quark density $x\Sigma^{\rm NNLO}(5, x, \mu^2)$, where $\sigma = (u + \bar{u})/2$, in the range $10^{-5} < x < 1$ for the same scales. Also in this case the ratios of the evolved densities to the FOPT densities is very close to unity for all x and μ^2 values so we do not show any plot. In Fig.9(b) we show the corresponding three-flavor NLO density.

In Fig.10(a) we show the nonsinglet quark density $x\sigma^{\rm NNLO}(5, x, \mu^2)$ in the range $10^{-5} < x < 1$ for the same scales. Also in this case the ratios of the evolved densities to the FOPT densities is very close to unity for all x and μ^2 values so we do not show any plot. In Fig.10(b) we show the corresponding three-flavor NLO density.

In Fig.11(a) we show the strange quark density $xs^{\rm NNLO}(5, x, \mu^2)$ in the range $10^{-5} < x < 1$ for the same scales. Also in this case the ratios of the evolved densities to the FOPT densities is very close to unity for all x and μ^2 values so we do not show any plot. In Fig.11(b) we show the corresponding three-flavor NLO density. We have checked that the five-flavour densities satisfy the momentum sum rule.

The above plots demonstrate that the NNLO matching conditions do influence the parton densities appreciably in regions just above $\mu = m_c$ and $\mu = m_b$. This has consequences for the analysis of HERA experiments because a lot of the data is at small x and small values of the scale Q^2. In fact all of the data for $x < 10^{-4}$ has $Q^2 < 100$ $(\mathrm{GeV/c^2})^2$. Even for the scale μ much larger than m_b the boundary conditions are still important. For $\mu \geq 10$ $\mathrm{GeV/c^2}$ for example the rapid rise of the five-flavour gluon density means that it dominates over all the other parton densities at small x. There is roughly a ten percent difference between the three-flavor and five-flavor densities at small x and large μ^2, which can be important for precision phenomenology.

ACKNOWLEDGMENTS

This research was partially supported by the National Science Foundation grant PHY-9722101. We thank M. Botje, E. Laenen and W.L. van Neerven for very useful discussions.

Appendix A

All the splitting functions in the Altarelli-Parisi (AP) equations can be expanded as a perturbation series in α_s into LO and NLO terms as follows

$$P = P^{(0)} + \frac{\alpha_s}{2\pi} P^{(1)}. \tag{A.1}$$

The non-singlet combinations of the $q_r(\bar{q}_r)$ to $q_s(\bar{q}_s)$ splitting functions, where the subscripts r, s denote the flavors of the (anti)quarks and satisfies $r, s = 1, \cdots, n_f$, can be further decomposed into a flavor diagonal part proportional to δ_{rs} and a flavor independent part. In LO there is only one non-singlet splitting function P_{qq} but in NLO it is convenient to form two combinations from P_{qq} and $P_{q\bar{q}}$ as follows

$$\begin{aligned} P_+ &= P_{qq} + P_{q\bar{q}} \\ P_- &= P_{qq} - P_{q\bar{q}}. \end{aligned} \tag{A.2}$$

These splitting functions are used to evolve two independent types of non-singlet densities, which will be called plus and minus respectively. They are given by

$$\begin{aligned} f_i^+ &= f_q^{\rm NS}(n_f, x, \mu^2) \\ f_j^- &= f_{k-\bar{k}}(n_f, x, \mu^2). \end{aligned} \tag{A.3}$$

The easiest way to explain the indices in these equations is by explicitly giving the combinations we use. For $j = 1, 2$

$$f_1^- = u - \bar{u}\,,\; f_2^- = d - \bar{d}\,, \tag{A.4}$$

which are used for all flavour density sets. Then for three-flavor densities $i = 1, 2, 3$ and we define

$$\begin{aligned} f_1^+ &= u + \bar{u} - \Sigma(3)/3\,, \qquad f_2^+ = d + \bar{d} - \Sigma(3)/3\,, \\ f_3^+ &= s + \bar{s} - \Sigma(3)/3\,, \end{aligned} \tag{A.5}$$

where $\Sigma(3) = f_q^S(3) = u + \bar{u} + d + \bar{d} + s + \bar{s}$. These densities should be used for $\mu < m_c$. For four-flavor densities $i = 1, 2, 3, 4$ and we define

$$\begin{aligned} f_1^+ &= u + \bar{u} - \Sigma(4)/4\,, \qquad f_2^+ = d + \bar{d} - \Sigma(4)/4\,, \\ f_3^+ &= s + \bar{s} - \Sigma(4)/4\,, \qquad f_4^+ = c + \bar{c} - \Sigma(4)/4\,, \end{aligned} \tag{A.6}$$

where $\Sigma(4) = f_q^S(4) = c + \bar{c} + \Sigma(3)$. These should be used for $m_c \leq \mu < m_b$. For five-flavor densites $i = 1, 2, 3, 4, 5$ and we define

$$\begin{aligned} f_1^+ &= u + \bar{u} - \Sigma(5)/5\,, \qquad f_2^+ = d + \bar{d} - \Sigma(5)/5\,, \\ f_3^+ &= s + \bar{s} - \Sigma(5)/5\,, \qquad f_4^+ = c + \bar{c} - \Sigma(5)/5\,, \\ f_5^+ &= b + \bar{b} - \Sigma(5)/5\,, \end{aligned} \tag{A.7}$$

where $\Sigma(5) = f_S^q(5) = b + \bar{b} + \Sigma(4)$. These should be used for $\mu \geq m_b$.

If we define $t = \ln(\mu^2/(1(\mathrm{GeV/c}^2)^2)$ then the AP equations that we need to solve are

$$\frac{\partial f_i^+(x,t)}{\partial t} = \frac{\alpha_s(t)}{2\pi}\int_x^1 \frac{dz}{z} P_+(\frac{x}{z}) f_i^+(z,t)\,, \tag{A.8}$$

$$\frac{\partial f_j^-(x,t)}{\partial t} = \frac{\alpha_s(t)}{2\pi}\int_x^1 \frac{dz}{z} P_-(\frac{x}{z}) f_j^-(z,t)\,, \tag{A.9}$$

$$\frac{\partial f_g(x,t)}{\partial t} = \frac{\alpha_s(t)}{2\pi}\int_x^1 \frac{dz}{z}\left[P_{gq}(\frac{x}{z}) f_q^S(z,t) + P_{gg}(\frac{x}{z}) f_g^S(z,t)\right]\,, \tag{A.10}$$

$$\frac{\partial f_q^S(x,t)}{\partial t} = \frac{\alpha_s(t)}{2\pi}\int_x^1 \frac{dz}{z}\left[P_{qq}(\frac{x}{z}) f_q^S(z,t) + P_{qg}(\frac{x}{z}) f_g^S(z,t)\right]\,, \tag{A.11}$$

where for $\mu < m_c$ we set $i = 1, 2, 3$, $j = 1, 2$, $f_q^S = \Sigma(3)$ and the gluon is a three-flavor gluon. When $m_c \leq \mu < m_b$, we use $i = 1, 2, 3, 4$, $j = 1, 2$, $f_q^S = \Sigma(4)$ and the gluon is a four-flavor gluon. Finally when $\mu \geq m_b$, we set $i = 1, 2, 3, 4, 5$, $j = 1, 2$, $f_q^5 = \Sigma(5)$ and the gluon is a five-flavor gluon.

The densities should satisfy the momentum conservation sum rule

$$\begin{aligned} &\int_0^1 x\left[u(x,\mu^2) + d(x,\mu^2) + \bar{u}(x,\mu^2) + \bar{d}(x,\mu^2) + 2s(x,\mu^2)\right. \\ &\left.+2c(x,\mu^2)\theta(\mu^2 - m_c^2) + 2b(x,\mu^2)\theta(\mu^2 - m_b^2) + g(x,\mu^2)\right]\, dx = 1\,. \end{aligned} \tag{A.12}$$

As the quark constituents carry all the charge, isospin, strange, charm and bottom quantum numbers of the nucleon they should also satisfy the other standard sum rules for the conservation of these quantities.

There are several methods to solve these equations. Among them the most popular are to use Mellin moments (used by [23], [24], see full list of references in [18] and [17]) and to use the direct x-space solution (as in [21], [17],[24], see also [18]). Also the authors in [22] describe a method involving Laguerre polynomials, that dates back to early paper of [5].

Our choice of direct x-space method is justified by the necessity to step densities across matching points using LO, NLO and NNLO boundary conditions. The procedure of doing this in the Mellin moment method would involve converting densities to and from Mellin moments several times. Using the direct x-space method is much more intuitive and straightforward. The main features of this method are linear interpolation over a grid in x and second-order interpolation over a grid in t. Let us describe the method in more detail to point out where we differ from the work in [17].

First we consider the x-variable in the evolution. Consider the right-hand-side of the evolution equation (A.8) for non-singlet density

$$I(x_0) = \int \frac{dz}{z} \frac{x_0}{z} P\left(\frac{x_0}{z}\right) q\left(z\right) \,, \tag{A.13}$$

where $x_0 \leq z \leq 1$ and

$$q(x) = xf(x) \,, \tag{A.14}$$

and

$$x_0 < x_1 < ... < x_n < x_{n+1} \equiv 1 \,, \tag{A.15}$$

with $q(x_{n+1}) = q(1) \equiv 0$. Between grid points x_i and x_{i+1}, x is chosen so that

$$q(x) = (1-y)q(x_i) + yq(x_{i+1}) \,, \tag{A.16}$$

with $y = (x - x_i)/(x_{i+1} - x_i)$. Using this relation we convert the integral into a sum

$$I(x_0) = \sum_{i=0}^{n+1} w(x_i, x_0) q(x_i) \,, \tag{A.17}$$

where the weights are

$$\begin{aligned} w(x_0, x_0) &= S_1(s_1, s_0) \\ w(x_i, x_0) &= S_1(s_{i+1}, s_i) - S_2(s_i, s_{i-1}) \,, \end{aligned} \tag{A.18}$$

where $s_i = x_0/x_i$ and

$$\begin{aligned} S_1(u,v) &= \frac{v}{v-u}\int_u^v (z-u)P(z)\frac{dz}{z} \\ S_2(u,v) &= \frac{u}{v-u}\int_u^v (z-v)P(z)\frac{dz}{z}\,. \end{aligned} \tag{A.19}$$

We have calculated these integrals analytically and the results are in the computer program. This leads to the final formula describing the grid for the x variable. Note that the weights $w^{(0)}$ and $w^{(1)}$ include LO and NLO splitting functions respectively. Thus, for the singlet case, we have

$$\begin{aligned} \frac{d(x_0\Sigma(x_0))}{dt} &= \frac{\alpha_s}{2\pi}\sum\left[w_{qq}^{(0)}(x_i,x_0)+\frac{\alpha_s}{2\pi}w_{qq}^{(1)}(x_i,x_0)\right]x_i\Sigma(x_i) \\ &\quad +\left[w_{qg}^{(0)}(x_i,x_0)+\frac{\alpha_s}{2\pi}w_{qg}^{(1)}(x_i,x_0)\right]x_i g(x_i)\,. \end{aligned} \tag{A.20}$$

Now consider the variation in the variable t. For each x_i we pick a grid in t labelled by distinct points t_j. Then the example the non-singlet equation becomes

$$q^{'}(x_i,t_j) = \frac{\alpha_s(t_j)}{2\pi}\sum_{k=1}^{n}\left[w_{\pm}^{(0)}(x_k,x_i)+\frac{\alpha_s(t_j)}{2\pi}w_{\pm}^{(1)}(x_k,x_i)\right]q(x_k,t_j)\,, \tag{A.21}$$

where $q^{'}(x_i,t_j)$ denotes the derivative with respect to t evaluated at $t=t_j$. In compact notation this equation can be rewritten as

$$q_j^{'} = wq_j + S\,, \tag{A.22}$$

with S being the sum of the terms on the right hand side of (A.21) excluding the j-th term.

For t between the grid points t_{j-1} and t_j we interpolate the parton density using quadratic interpolation as follows

$$q(x_i,t) = at^2+bt+c\,. \tag{A.23}$$

Thus we relate the value of q at the point t_j to that of q at the point t_{j-1} by

$$q(x_i,t_j) = q(x_i,t_{j-1}) + \frac{1}{2}[q^{'}(x_i,t_j)+q^{'}(x_i,t_{j-1})]\Delta t_j\,, \tag{A.24}$$

where $\Delta t_j = t_j - t_{j-1}$. This equation can also be written more compactly as

$$q_j = q_{j-1} + \frac{1}{2}(q_{j-1}^{'} + q_j^{'})\Delta t_j \,. \tag{A.25}$$

The resulting system of two linear equations (A.25) and (A.22) for q_j and $q_j^{'}$ has the solution

$$q_j = \frac{2q_{j-1} + (q_{j-1}^{'} + S)\Delta t_j}{2 - w\Delta t_j} \,, \tag{A.26}$$

and yields $q_j^{'}$ from (A.22). Applying the same procedure to the gluon and singlet equations Eqs.(A.10)-(A.11) involves four equations because we have to compute both the densities and their derivatives.

The evolution proceeds from the initial $\mu_0^2 = \mu_{\rm LO}^2$ (or $\mu_0^2 = \mu_{\rm NLO}^2$) to the first matching point at the scale $\mu^2 = m_c^2$. Next the charm density is introduced in the NNLO (α_s^2-order terms) and all the four-flavor densities are evolved from the boundary conditions in Ens.(2.8)-(2.10). This evolution continues up to the transition point $\mu^2 = m_b^2$, where the same procedure is applied to generate the bottom quark density. At that matching point all five-flavor densities are evolved starting from the boundary conditions in Eqs.(2.8)-(2.11) up to all higher μ^2 scales.

References

[1] H.L. Lai, J. Huston, S. Kuhlmann, J. Morfín, F. Olness, J. Owens, J. Pumplin and W.K. Tung, hep-ph/9903282.

[2] M. Glück, E. Reya and A. Vogt, Eur. Phys. J. **C5**, 461 (1998).

[3] A.D. Martin, R.G. Roberts, W.J. Stirling and R. Thorne, Eur. Phys. J. **C4**, 463 (1998).

[4] G. Altarelli and G. Parisi, Nucl. Phys. **B126**, 298 (1977).

[5] G. Curci, W. Furmanski and R. Petronzio, Nucl. Phys. **B175**, 27 (1980); W. Furmanski and R. Petronzio, Phys. Lett. **B97** 437, (1980); ibid. Z. Phys. **C11**, 293 (1982); the relevant NLO formulae are presented in a convenient form in R.K. Ellis, W.J. Stirling and B.R. Webber, in *QCD and Collider Physics,* Cambridge University Press (1996), Chapter 4.3.

[6] S.A. Larin, T. van Ritbergen and J.A.M. Vermaseren, Nucl. Phys. **B427**, 41 (1994); S.A. Larin et al., Nucl. Phys. **B492**, 338 (1997).

[7] W.L. van Neerven and A. Vogt, hep-ph/9907472.

[8] J.F. Bennett and J.A Gracey, Nucl. Phys. **B417**, 241 (1998); J.A. Gracey, Phys. Lett. **B322**, 141 (1994).

[9] C. Adloff et al. (H1-collaboration), Nucl. Phys. **B545**, 21 (1999).

[10] J. Breitweg et al. (ZEUS Collaboration), Phys. Lett. **B407**, 402 (1997), hep-ex/9908012.

[11] M.A.G. Aivazis, J.C. Collins, F.I. Olness and W.-K. Tung, Phys. Rev. D**50**, 3102 (1994); J.C. Collins, Phys. Rev. D**58**, 0940002 (1998).

[12] R.S. Thorne and R.G. Roberts, Phys. Lett. **B421**, 303 (1998); Phys. Rev. D**57**, 6871 (1998).

[13] M. Glück, E. Reya and M. Stratmann, Nucl. Phys. **B422**, 37 (1994); A. Vogt in *Deep Inelastic Scattering and Related Phenomena, DIS96*, edited by G.D. 'Agostini and A. Nigro, (World Scientific 1997), p. 254, hep-ph/9601352.

[14] E. Laenen, S. Riemersma, J. Smith and W.L. van Neerven, Nucl. Phys. **B392**, 162 (1993); ibid. 229 (1993); S. Riemersma, J. Smith and W.L. van Neerven, Phys. Lett. **B347**, 43 (1995); B.W. Harris and J. Smith, Nucl. Phys. **B452**, 109 (1995).

[15] M. Buza, Y. Matiounine, J. Smith and W.L. van Neerven, Eur. Phys. J. **C1**, 301 (1998).

[16] A. Chuvakin, J. Smith and W. van Neerven, hep-ph/9910250, YITP-SB-99-15, INLO-PUB-12/99, submitted to Phys. Rev. D.

[17] M. Botje, QCDNUM16: A fast QCD evolution program, ZEUS Note 97-066.

[18] J. Blümlein, S. Riemersma, W.L. van Neerven and A. Vogt, Nucl. Phys. **B**(Proc. Suppl.) **51C**, 96 (1996);
J. Blümlein et al., in *Proceedings of the Workshop on Future Physics at HERA* edited by G. Ingelman, A. De Roeck and R. Klanner, Hamburg, Germany, 25-26 Sep. 1995, p. 23, DESY 96-199, hep-ph/9609400.

[19] W. Bernreuther and W. Wetzel, Nucl. Phys. **B197**, 228 (1982); W. Bernreuther, Annals of Physics, **151**, 127 (1983).

[20] S.A. Larin, T. van Ritbergen and J.A.M. Vermaseren, Nucl. Phys. **B438**, 278 (1995); see also K.G. Chetyrkin, B.A. Kniehl and M. Steinhauser, Phys. Rev. Lett. **79**, 2184 (1997).

[21] M. Miyama and S. Kumano, Comput. Phys. Commun. **94**, 185 (1996); M. Hirai, S. Kumano and M. Miyama, Comput. Phys. Commun. **108**, 38 (1998).

[22] C. Coriano and S. Savkli, Comput. Phys. Commun. **118**, 236 (1999).

[23] S. Riemersma, unpublished.

[24] C. Pascaud and F. Zomer, H1 Note H1-11/94-404; V. Barone, C. Pascaud and F. Zomer, hep-ph/9907512.

Figure Captions

Fig. 1. (a) The charm quark density $xc_{\rm NNLO}(4,x,\mu^2)$ the range $10^{-5} < x < 1$ for $\mu^2 = 1.96$, 2, 3, 4, 5, 10 and 20 in units of $({\rm GeV/c}^2)^2$, (b) similar plot as in (a) but now for $0.01 < x < 1$, (c) ratios $R_c^{\rm NNLO}(x,\mu^2) = xc_{\rm EVOLVED}(4,x,\mu^2)/xc_{\rm FOPT}(4,x,\mu^2)$ for the same scales, (d) and (e) the NLO results from MRST98 set 1 and CTEQ5HQ respectively.

Fig. 2. (a) The gluon density $xg_{\rm NNLO}(4,x,\mu^2)$ in the range $10^{-5} < x < 1$ for $\mu^2 = 2$, 3, 4, 5, 10 and 20 in units of $({\rm GeV/c}^2)^2$, (b) ratios $R_g^{\rm NNLO}(x,\mu^2) = xg_{\rm EVOLVED}(4,x,\mu^2)/xg_{\rm FOPT}(4,x,\mu^2)$ for the same scales, (c) the three-flavor NLO gluon density in the same range, (d) and (e) the NLO results from MRST98 set 1 and CTEQ5HQ respectively.

Fig. 3. (a) The singlet density $x\Sigma_{\rm NNLO}(4,x,\mu^2)$ in the range $10^{-5} < x < 1$ for $\mu^2 = 2$, 3, 4, 5, 10 and 20 in units of $({\rm GeV/c}^2)^2$, (b) ratios $R_\Sigma^{\rm NNLO}(x,\mu^2) = x\Sigma_{\rm EVOLVED}(4,x,\mu^2)\ /x\Sigma_{\rm FOPT}(4,x,\mu^2)$ for the same scales, (c) the three-flavor NLO density.

Fig. 4. (a) The nonsinglet quark density $x\sigma_{\rm NNLO}(4,x,\mu^2)$ in the range $10^{-5} < x < 1$ for $\mu^2 = 2$, 3, 4, 5, 10 and 20 in units of $({\rm GeV/c}^2)^2$, (b) ratios $R_\sigma^{\rm NNLO}(x,\mu^2) = x\sigma_{\rm EVOLVED}(4,x,\mu^2)/x\sigma_{\rm FOPT}(4,x,\mu^2)$ for the same scales, (c) the three-flavor NLO density.

Fig. 5. (a) The strange quark density $xs_{\rm NNLO}(4,x,\mu^2)$ in the range $10^{-5} < x < 1$ for $\mu^2 = 2$, 3, 4, 5, 10 and 20 in units of $({\rm GeV/c}^2)^2$, (b) ratios $R_s^{\rm NNLO}(x,\mu^2) = xc_{\rm EVOLVED}(4,x,\mu^2)/xc_{\rm FOPT}(4,x,\mu^2)$ for the same scales, (c) the three-flavor NLO density.

Fig. 6. (a) The bottom quark density $xb_{\rm NNLO}(5,x,\mu^2)$ in the range $10^{-5} < x < 1$ for $\mu^2 = 20.25$, 25, 30, 40 and 100 in units of $({\rm GeV/c}^2)^2$, (b) similar plot as in (a) but now for $0.01 < x < 1$, (c) ratios $R_b^{\rm NNLO}(x,\mu^2) = xb_{\rm EVOLVED}(4,x,\mu^2)/xb_{\rm FOPT}(4,x,\mu^2)$ for the same scales, (d) and (e) the NLO results from MRST98 set 1 and CTEQ5HQ respectively.

Fig. 7. (a) The charm quark density $xc_{\rm NNLO}(5,x,\mu^2)$ in the range $10^{-5} < x < 1$ for $\mu^2 = 20.25$, 25, 30, 40 and 100 in units of $({\rm GeV/c}^2)^2$, (b) and (c) the NLO results from MRST98 set 1 and CTEQ5HQ respectively.

Fig. 8. (a) The gluon density $xg_{\rm NNLO}(5,x,\mu^2)$ in the range $10^{-5} < x < 1$ for $\mu^2 = 20.25$, 25, 30, 40 and 100 in units of $({\rm GeV/c^2})^2$, (b) the three-flavor NLO density.

Fig. 9. (a) The singlet quark density $x\Sigma_{\rm NNLO}(5,x,\mu^2)$ in the range $10^{-5} < x < 1$ for $\mu^2 = 20.25$, 25, 30, 40 and 100 in units of $({\rm GeV/c^2})^2$, (b) the three-flavor NLO density.

Fig. 10. (a) The nonsinglet density $x\sigma_{\rm NNLO}(5,x,\mu^2)$ in the range $10^{-5} < x < 1$ for $\mu^2 = 20.25$, 25, 30, 40 and 100 in units of $({\rm GeV/c^2})^2$, (b) the three-flavor NLO density.

Fig. 11. (a) The strange quark density $xs_{\rm NNLO}(5,x,\mu^2)$ in the range $10^{-5} < x < 1$ for $\mu^2 = 20.25$, 30, 40 and 100 in units of $({\rm GeV/c^2})^2$, (b) the three-flavor NLO density.

Fig 1(a)

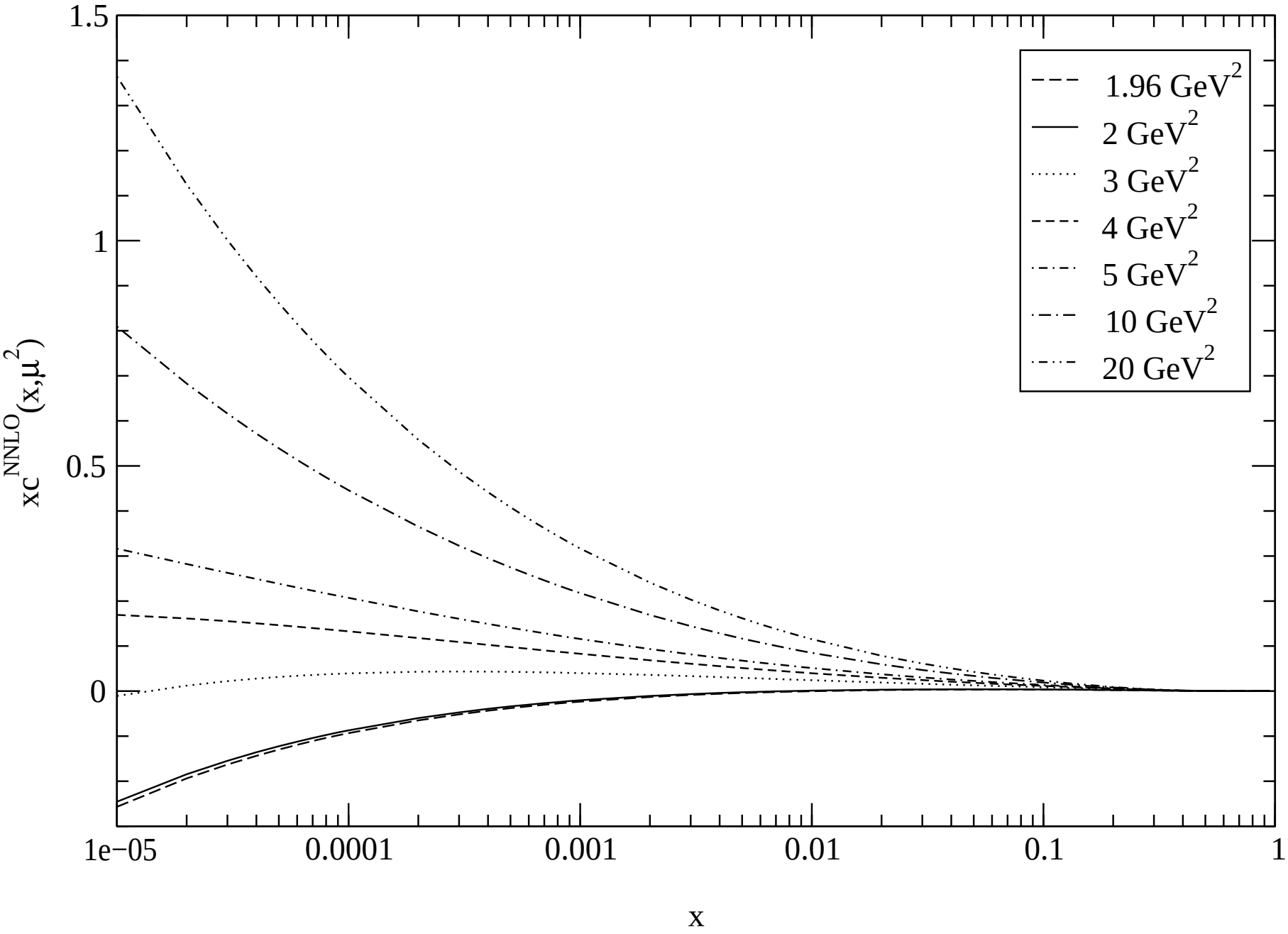
1.5
1
0.5
0
1e−05
0.0001
0.001
0.01
0.1
1
x
$xc^{NNLO}(x,\mu^2)$
1.96 GeV^2
2 GeV^2
3 GeV^2
4 GeV^2
5 GeV^2
10 GeV^2
20 GeV^2

Fig 1(b)

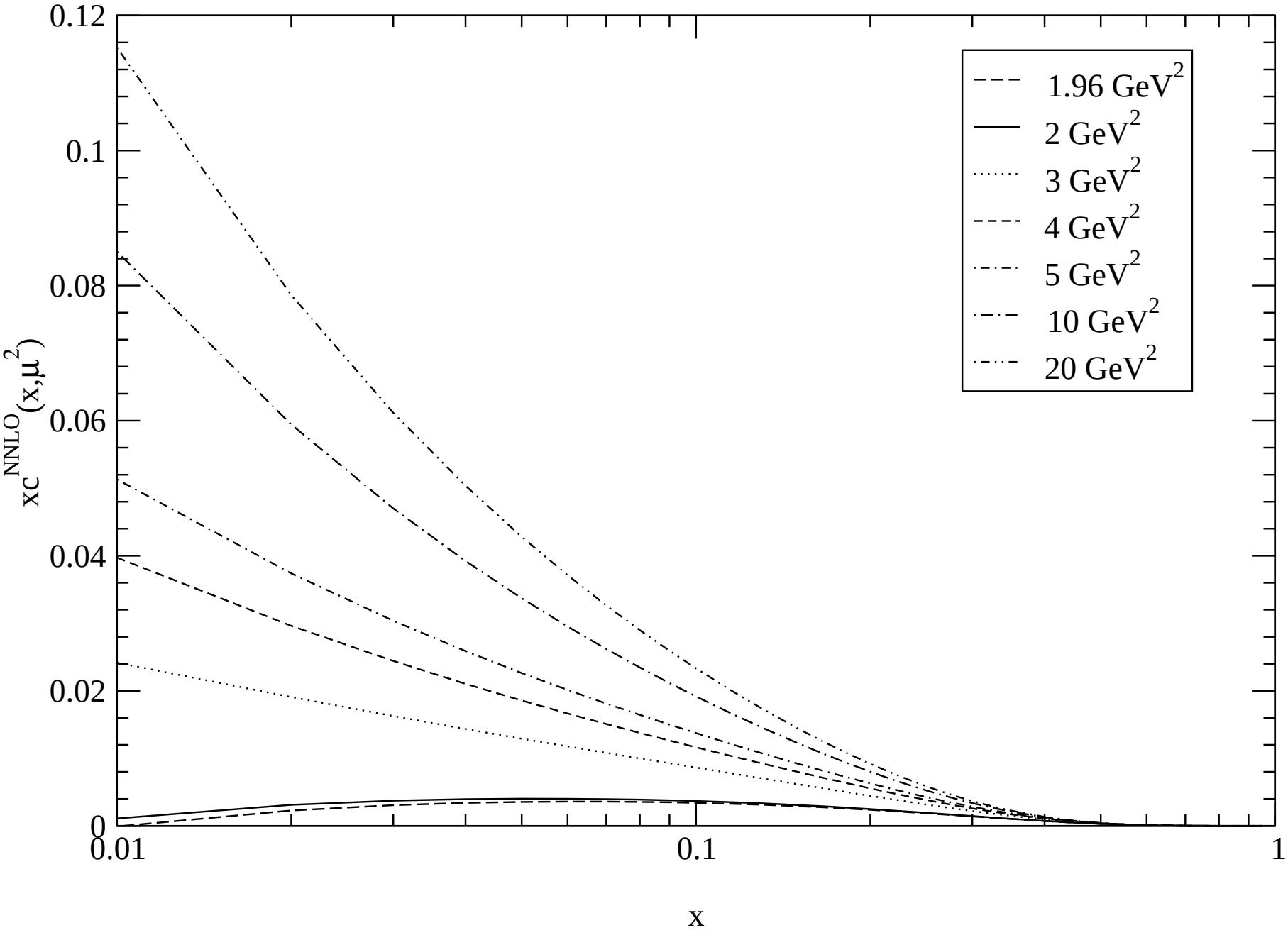
0.12
0.1
0.08
0.06
0.04
0.02
0
0.01
0.1
1
x
$xc^{NNLO}(x,\mu^2)$
1.96 GeV^2
2 GeV^2
3 GeV^2
4 GeV^2
5 GeV^2
10 GeV^2
20 GeV^2

Fig 1(c)

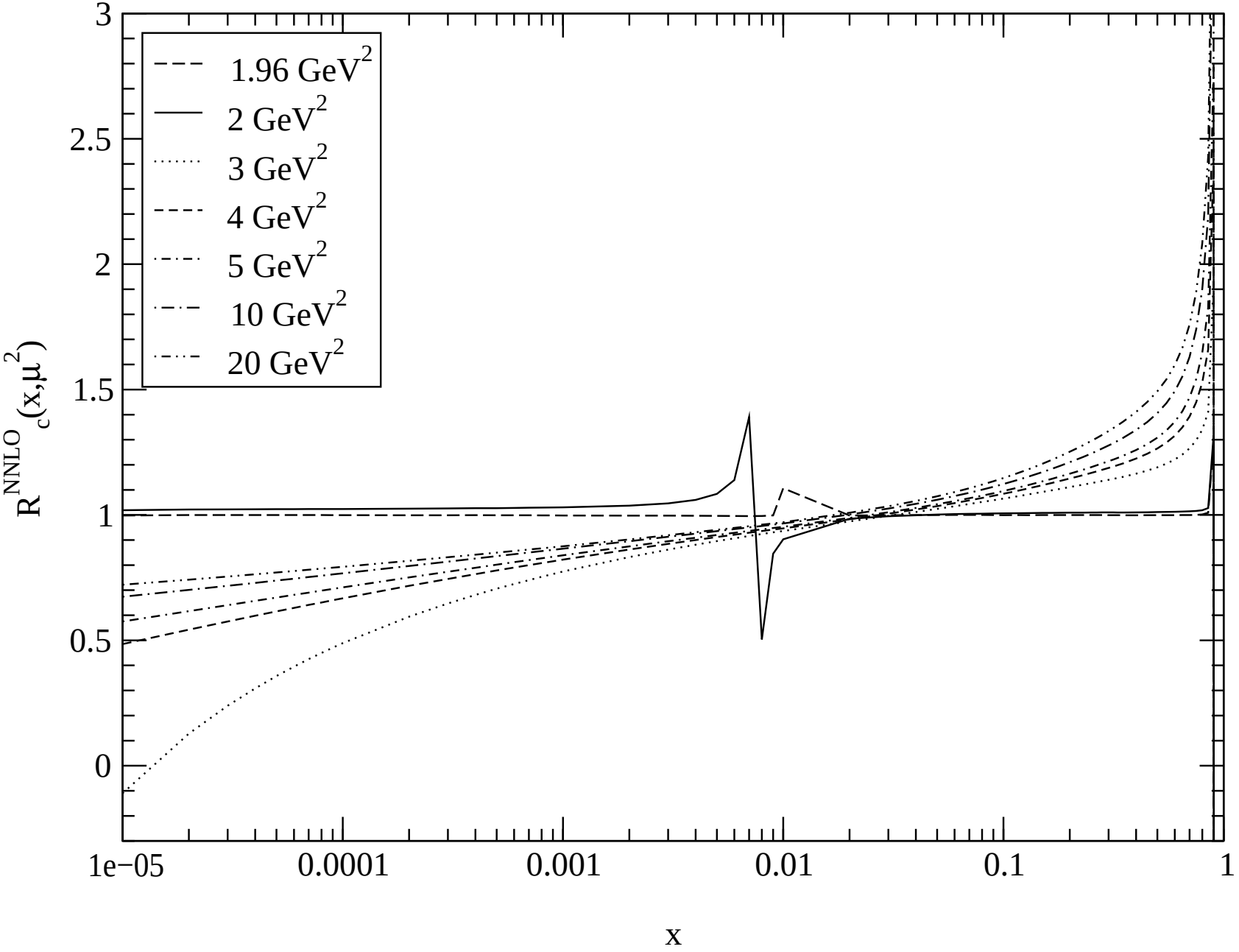
1.96 GeV^2
2 GeV^2
3 GeV^2
4 GeV^2
5 GeV^2
10 GeV^2
20 GeV^2
$R_c^{NNLO}(x,\mu^2)$
x
3
2.5
2
1.5
1
0.5
0
1e−05
0.0001
0.001
0.01
0.1
1

Fig 1(d)

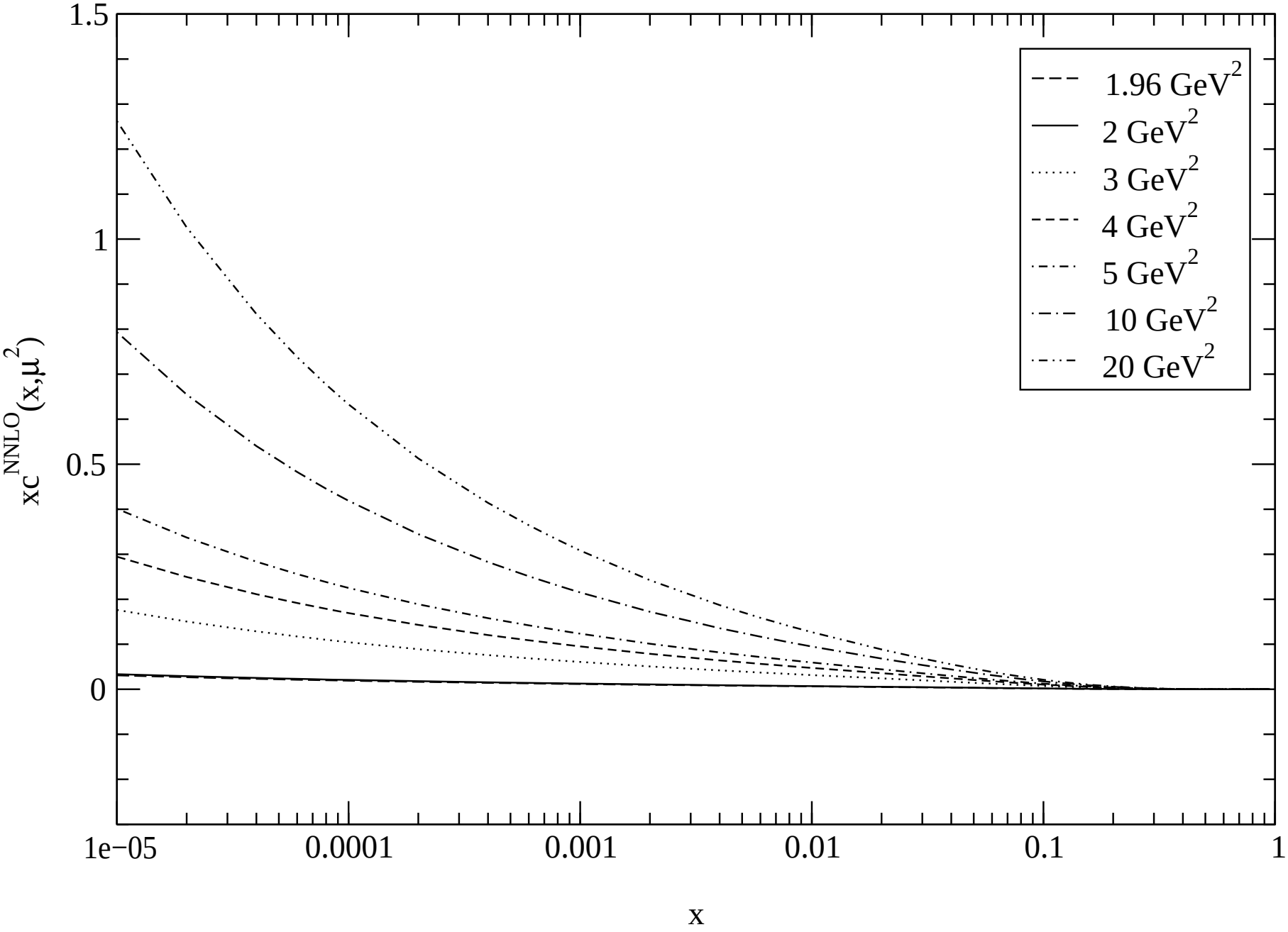
1.5
1
0.5
0
1e−05
0.0001
0.001
0.01
0.1
1
x
$xc^{NNLO}(x,\mu^2)$
1.96 GeV^2
2 GeV^2
3 GeV^2
4 GeV^2
5 GeV^2
10 GeV^2
20 GeV^2

Fig 1(e)

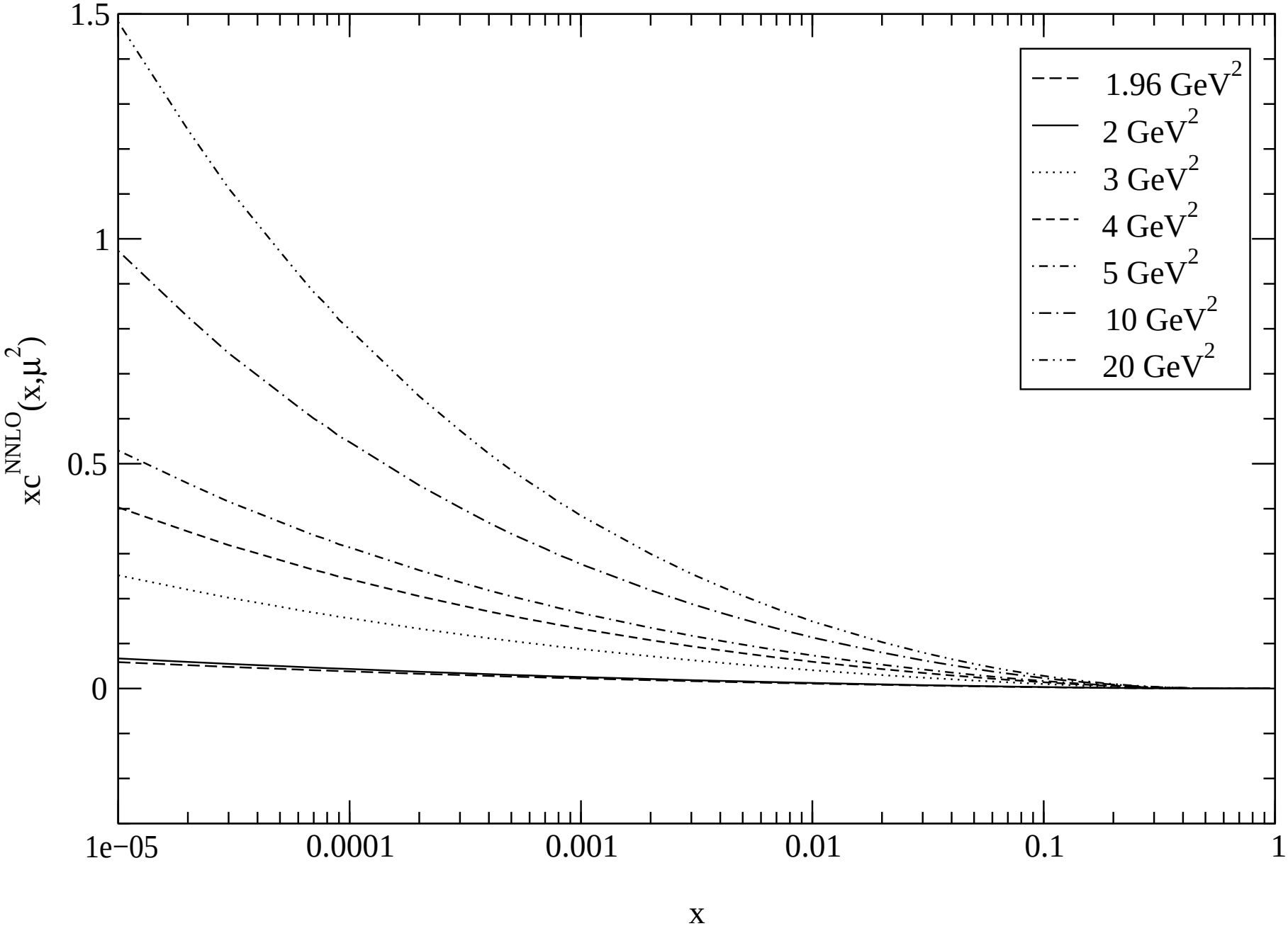
1.5
1
0.5
0
1e−05
0.0001
0.001
0.01
0.1
1
x
$xc^{NNLO}(x,\mu^2)$
1.96 GeV^2
2 GeV^2
3 GeV^2
4 GeV^2
5 GeV^2
10 GeV^2
20 GeV^2

Fig. 2(a)

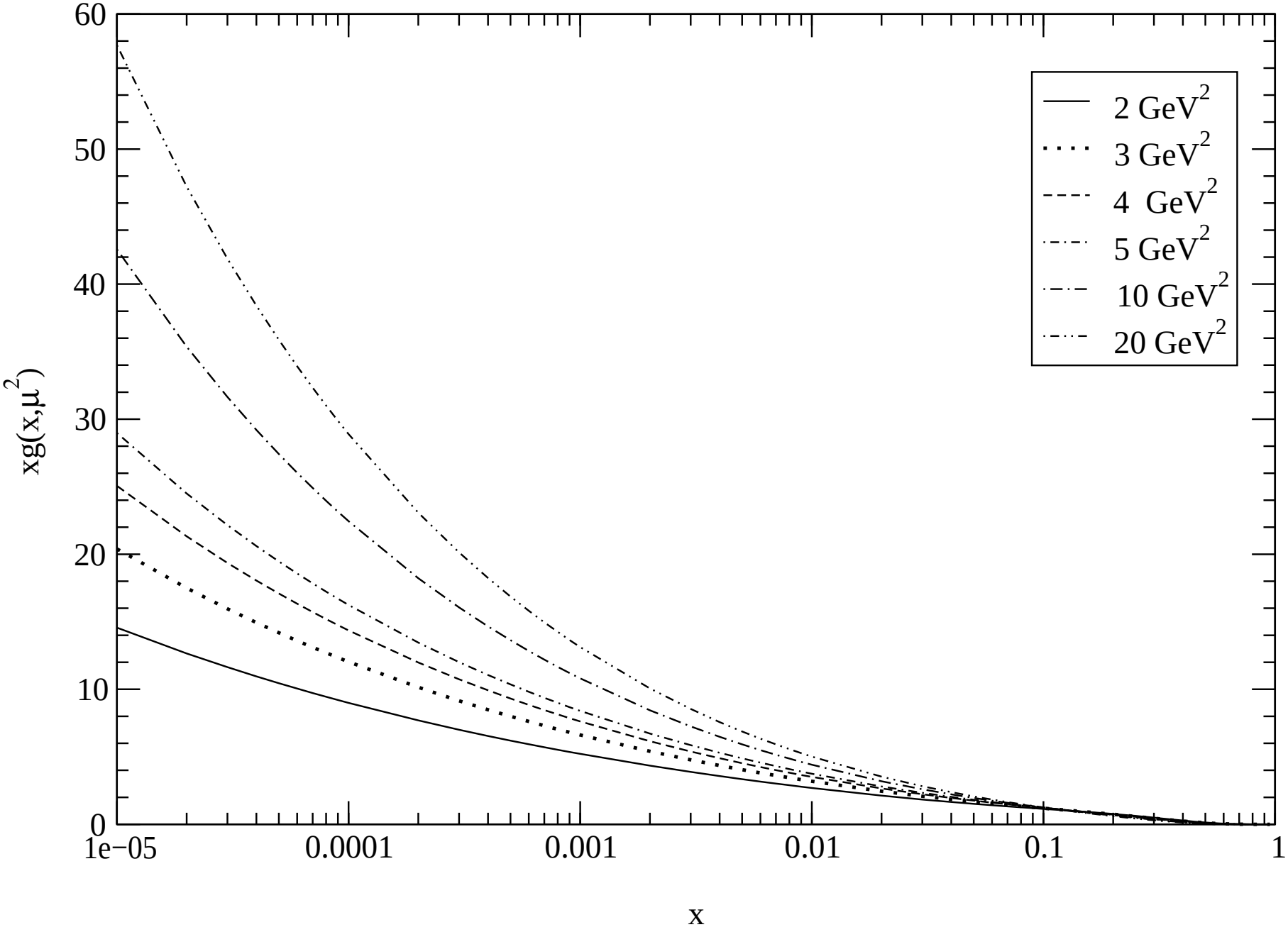
60
50
40
30
20
10
0
1e−05
0.0001
0.001
0.01
0.1
1
xg(x,μ2)
x
2 GeV2
3 GeV2
4 GeV2
5 GeV2
10 GeV2
20 GeV2

Fig. 2(b)

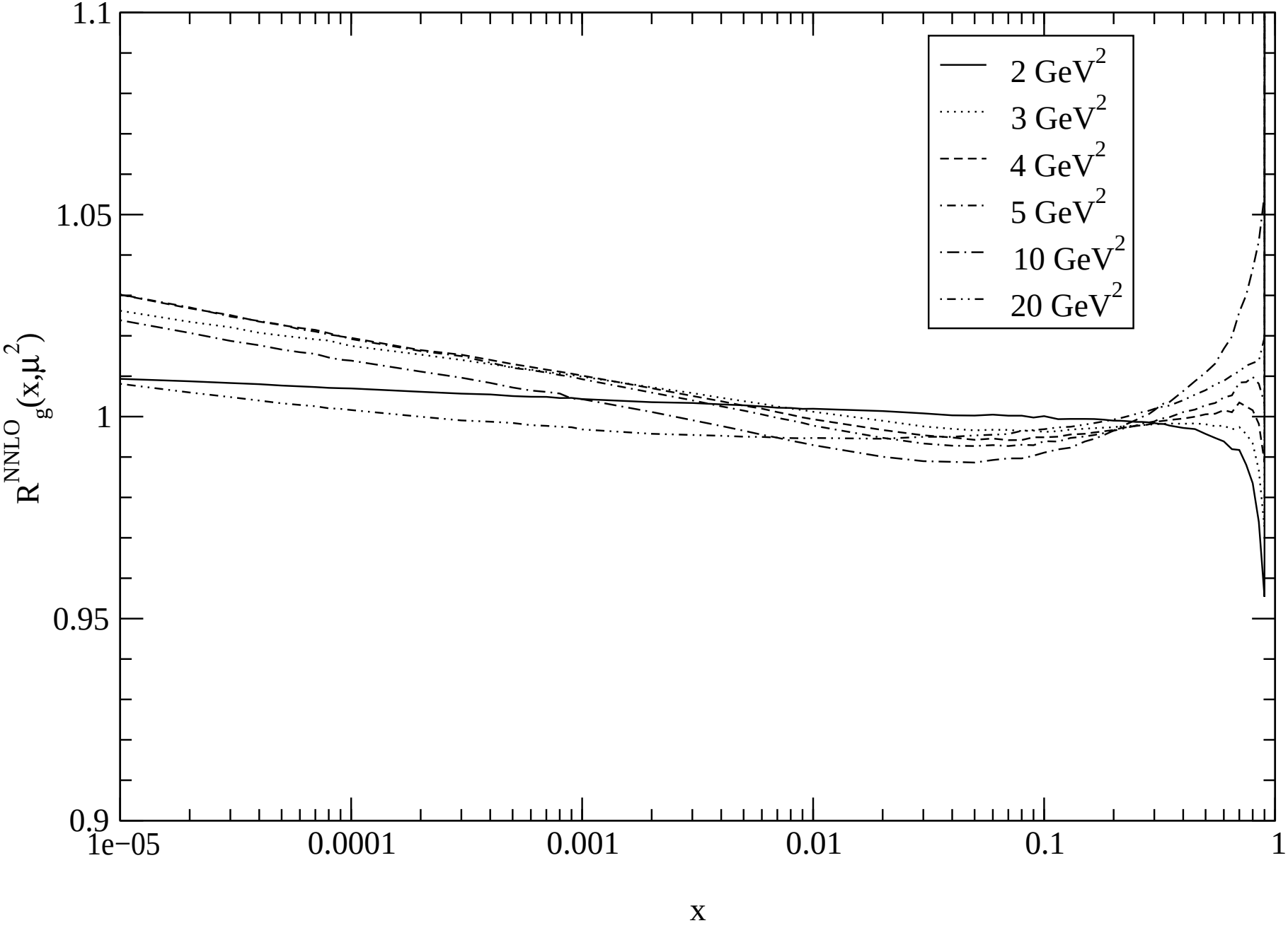
1.1
1.05
1
0.95
0.9
1e−05
0.0001
0.001
0.01
0.1
1
x
$R^{NNLO}_g(x,\mu^2)$
2 GeV^2
3 GeV^2
4 GeV^2
5 GeV^2
10 GeV^2
20 GeV^2

Fig. 2(c)

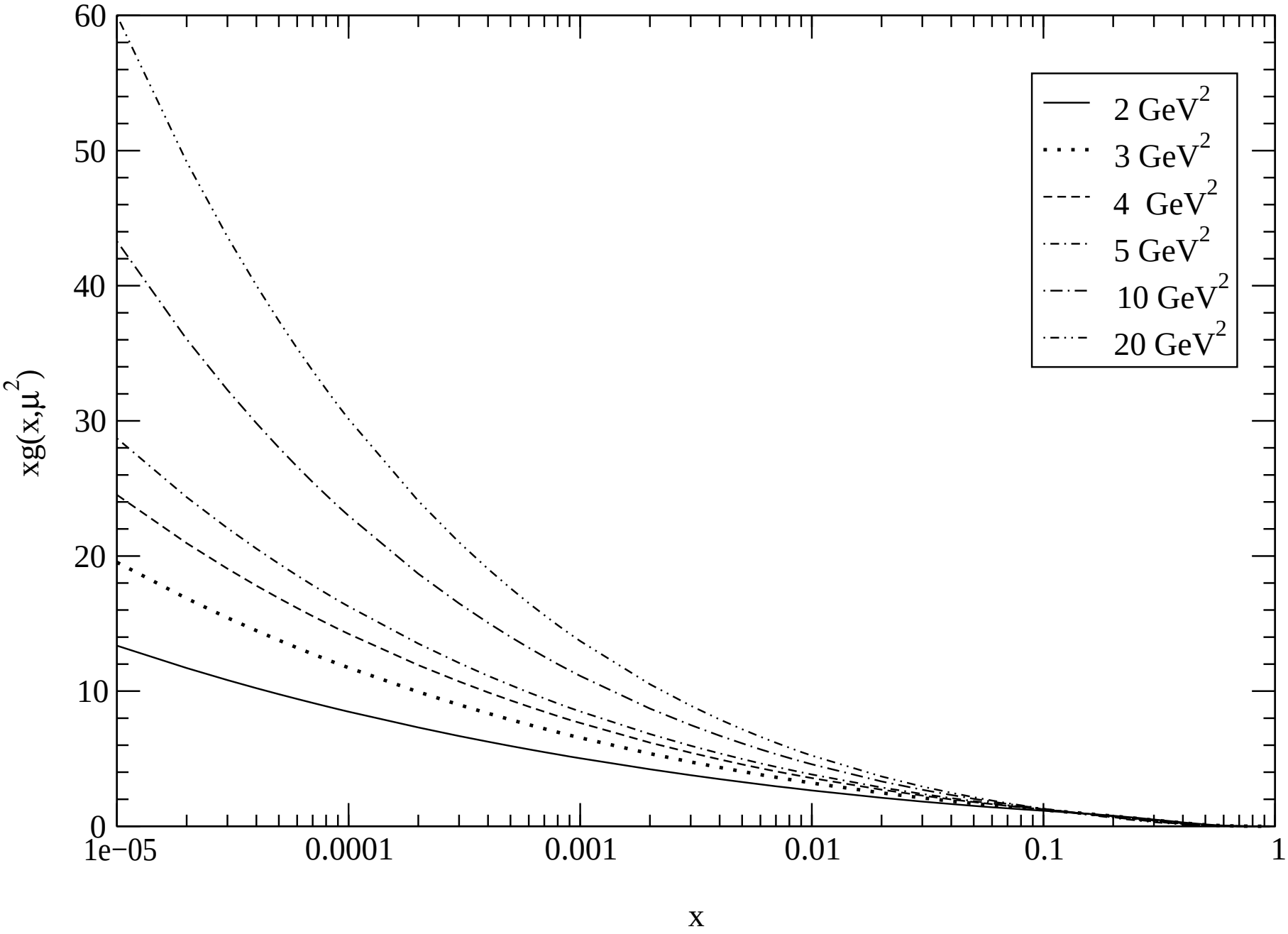
60
50
40
30
20
10
0
1e−05
0.0001
0.001
0.01
0.1
1
xg(x,μ2)
x
2 GeV2
3 GeV2
4 GeV2
5 GeV2
10 GeV2
20 GeV2

Fig. 2(d)

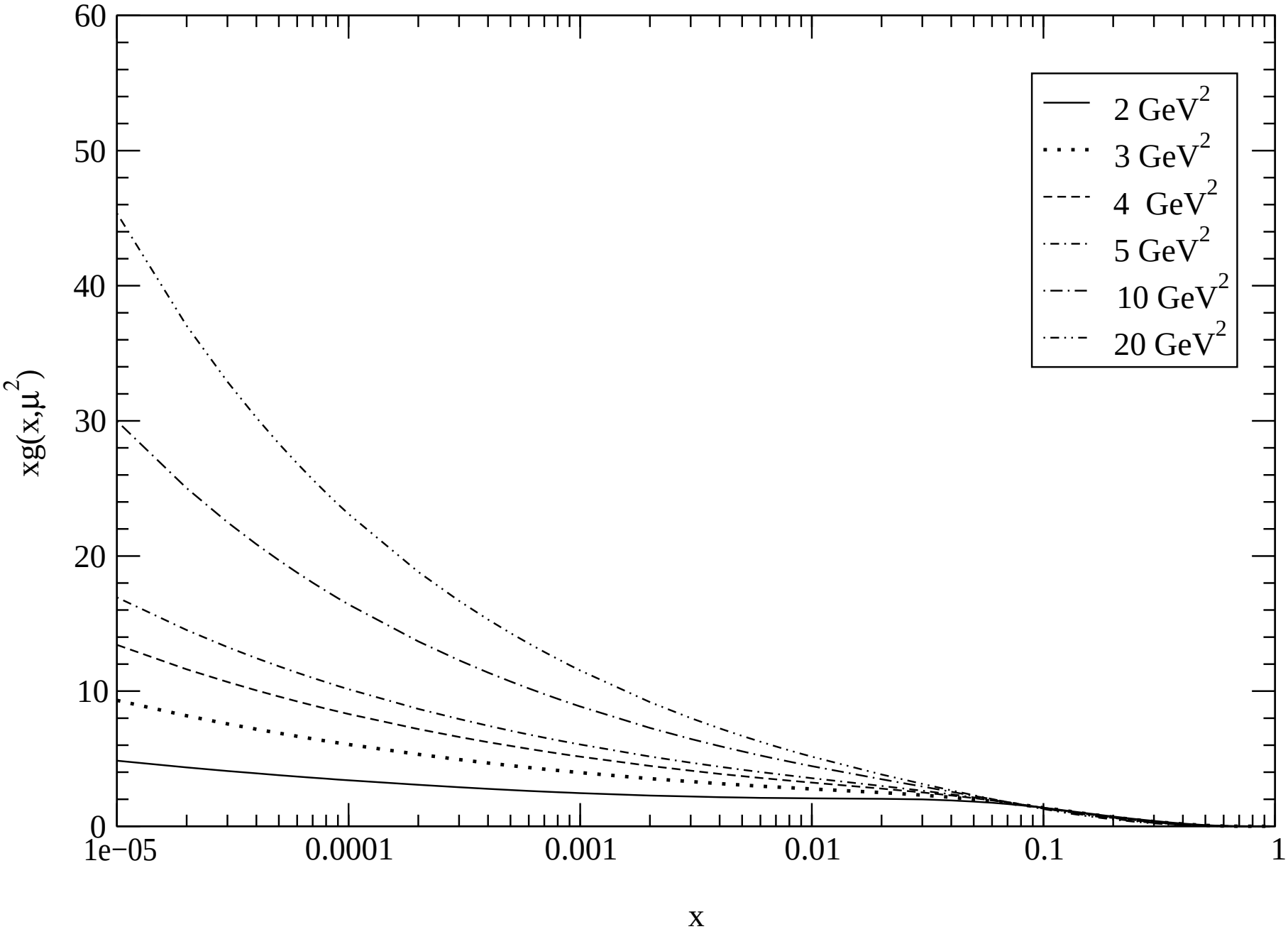
60
50
40
30
20
10
0
1e−05
0.0001
0.001
0.01
0.1
1
xg(x,μ2)
x
2 GeV2
3 GeV2
4 GeV2
5 GeV2
10 GeV2
20 GeV2

Fig. 2(e)

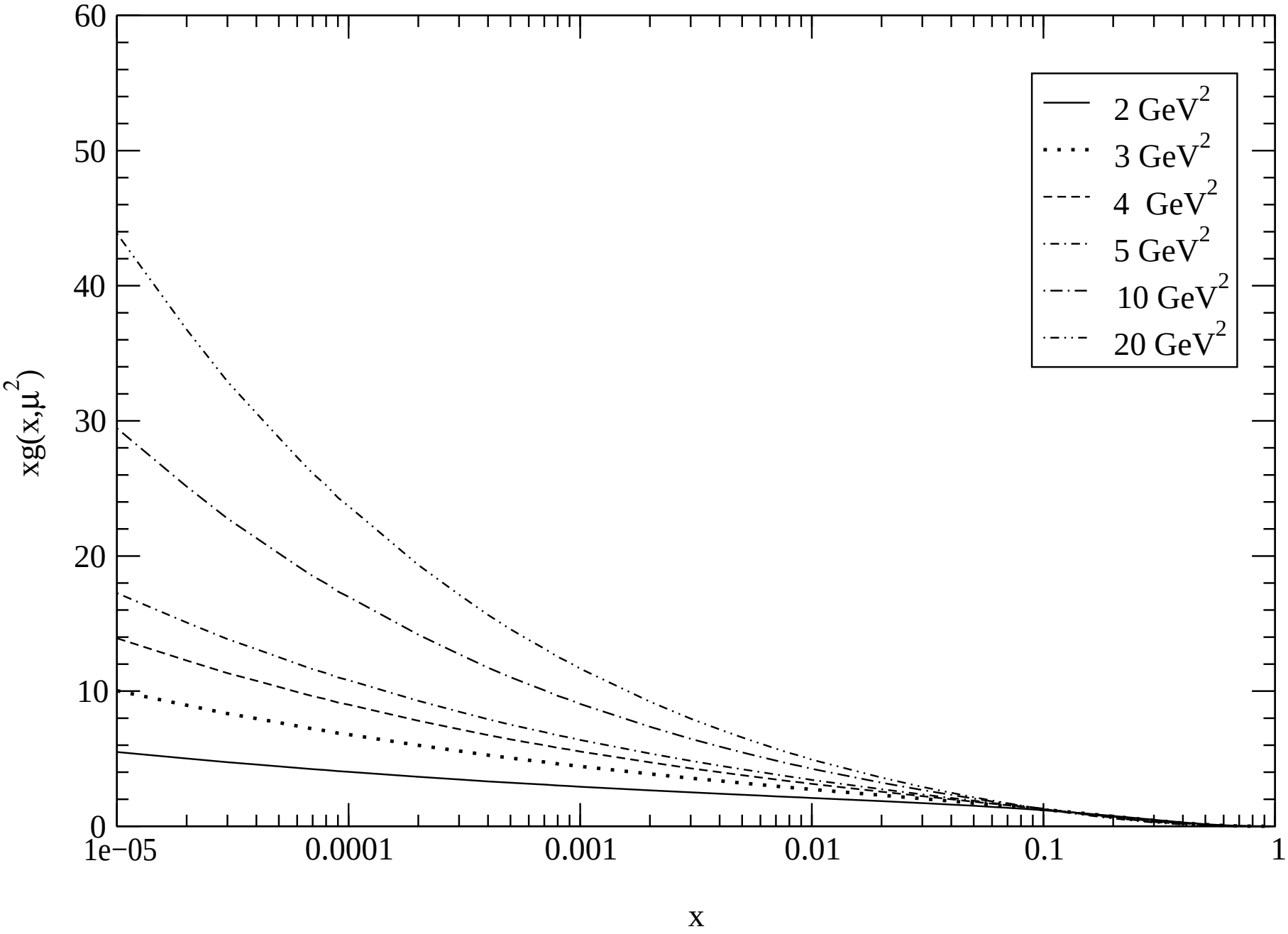
60
50
40
30
20
10
0
1e−05
0.0001
0.001
0.01
0.1
1
xg(x,μ2)
x
2 GeV2
3 GeV2
4 GeV2
5 GeV2
10 GeV2
20 GeV2

Fig. 3(a)

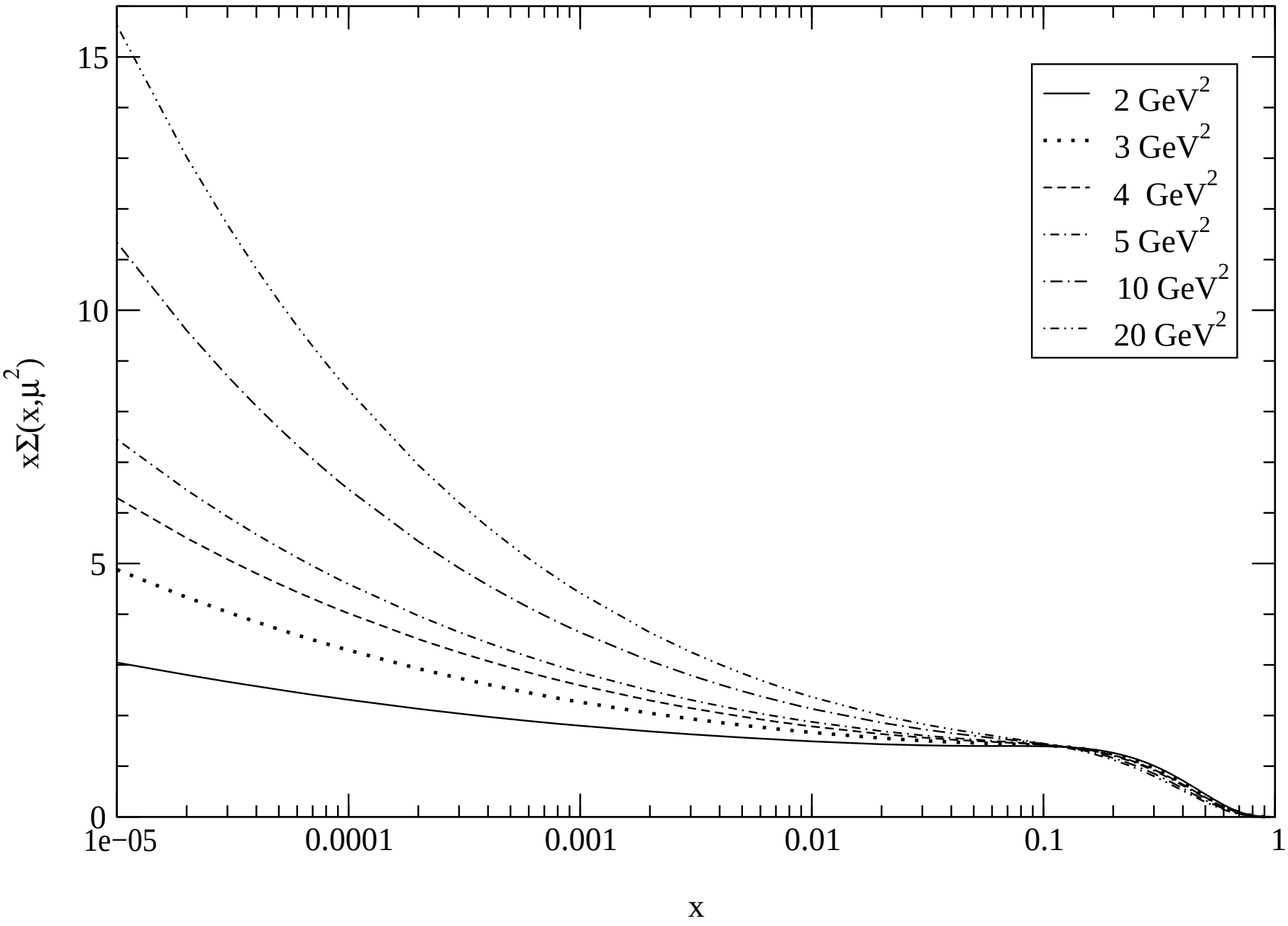
15
10
5
0
1e−05
0.0001
0.001
0.01
0.1
1
x
xΣ(x,μ2)
2 GeV2
3 GeV2
4 GeV2
5 GeV2
10 GeV2
20 GeV2

Fig. 3(b)

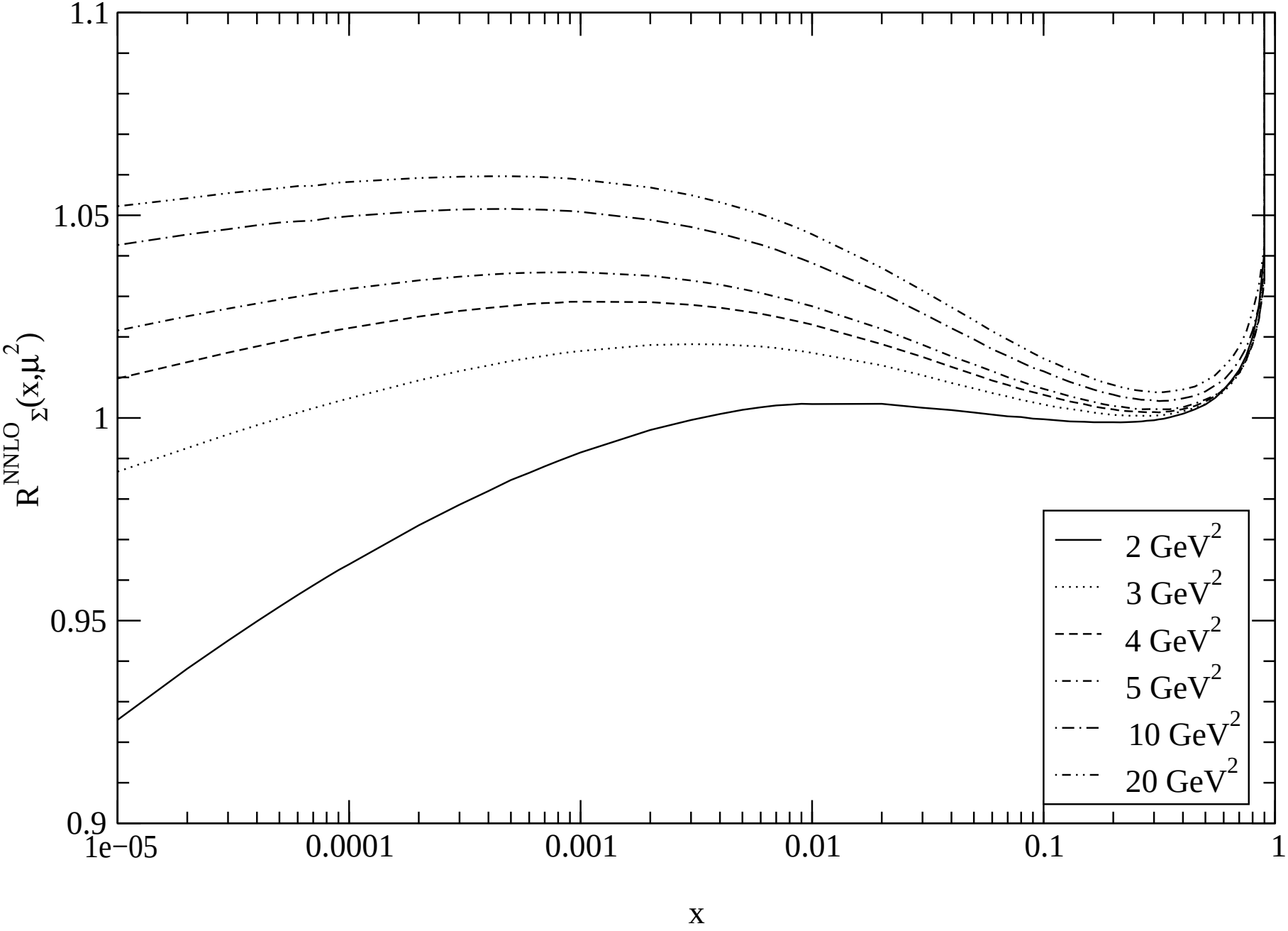
1.1
1.05
1
0.95
0.9
1e−05
0.0001
0.001
0.01
0.1
1
x
$R^{NNLO}_{\Sigma}(x,\mu^2)$
2 GeV^2
3 GeV^2
4 GeV^2
5 GeV^2
10 GeV^2
20 GeV^2

Fig. 3(c)

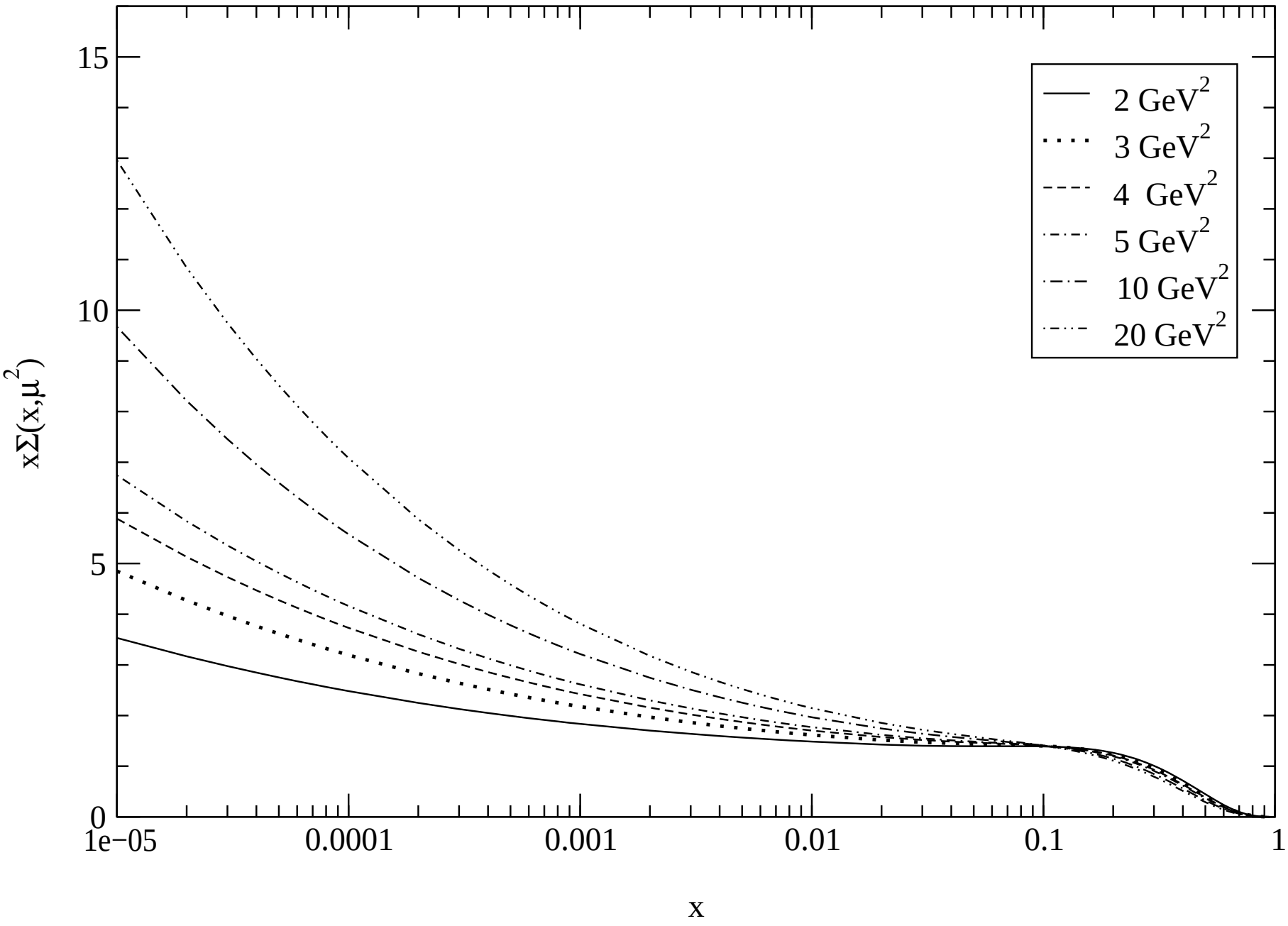
15
10
5
0
1e−05
0.0001
0.001
0.01
0.1
1
x
xΣ(x,μ2)
2 GeV2
3 GeV2
4 GeV2
5 GeV2
10 GeV2
20 GeV2

Fig. 4(a)

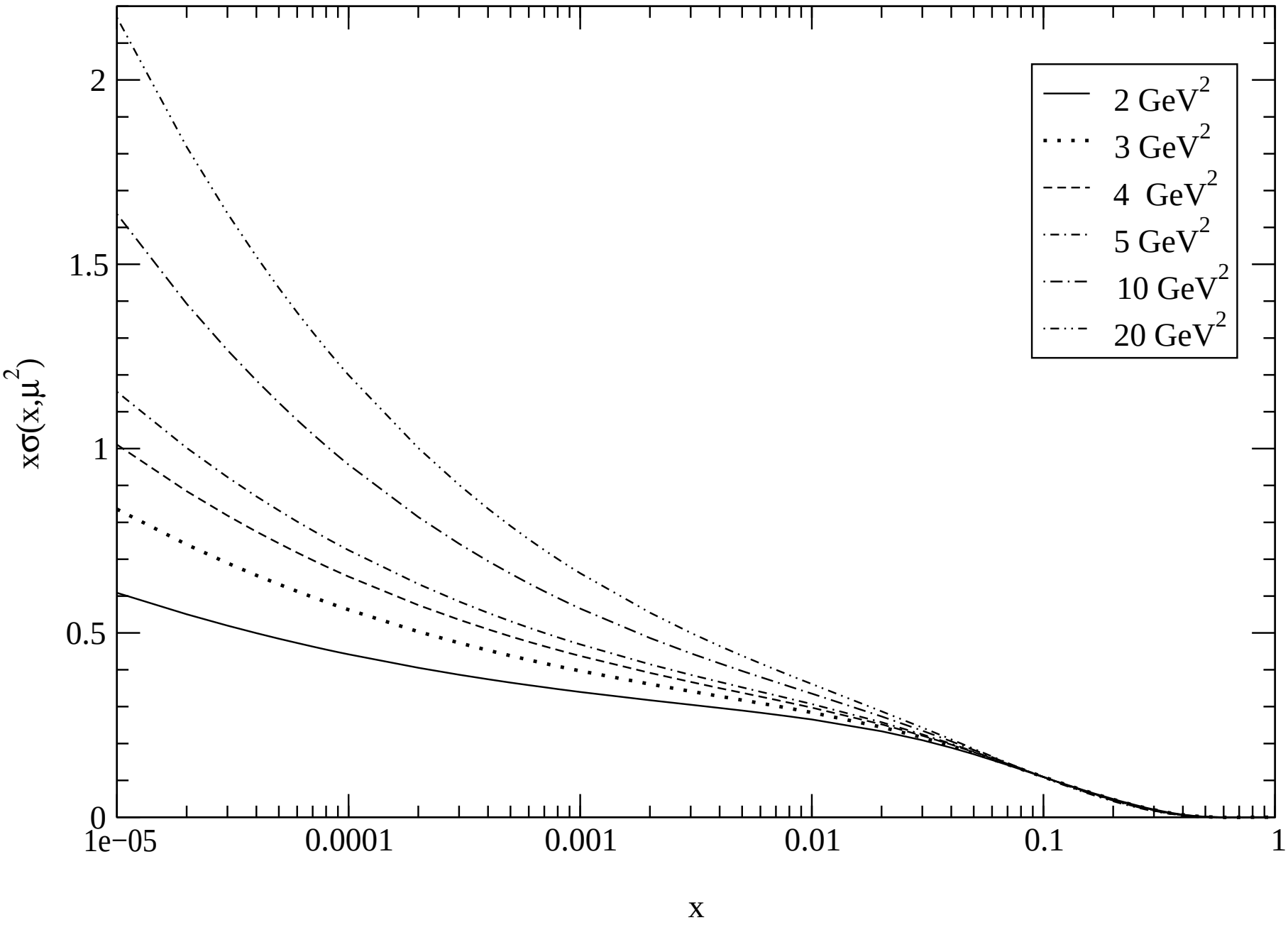
2 GeV^2
3 GeV^2
4 GeV^2
5 GeV^2
10 GeV^2
20 GeV^2
xσ(x,μ^2)
x
0
0.5
1
1.5
2
1e−05
0.0001
0.001
0.01
0.1
1

Fig. 4(b)

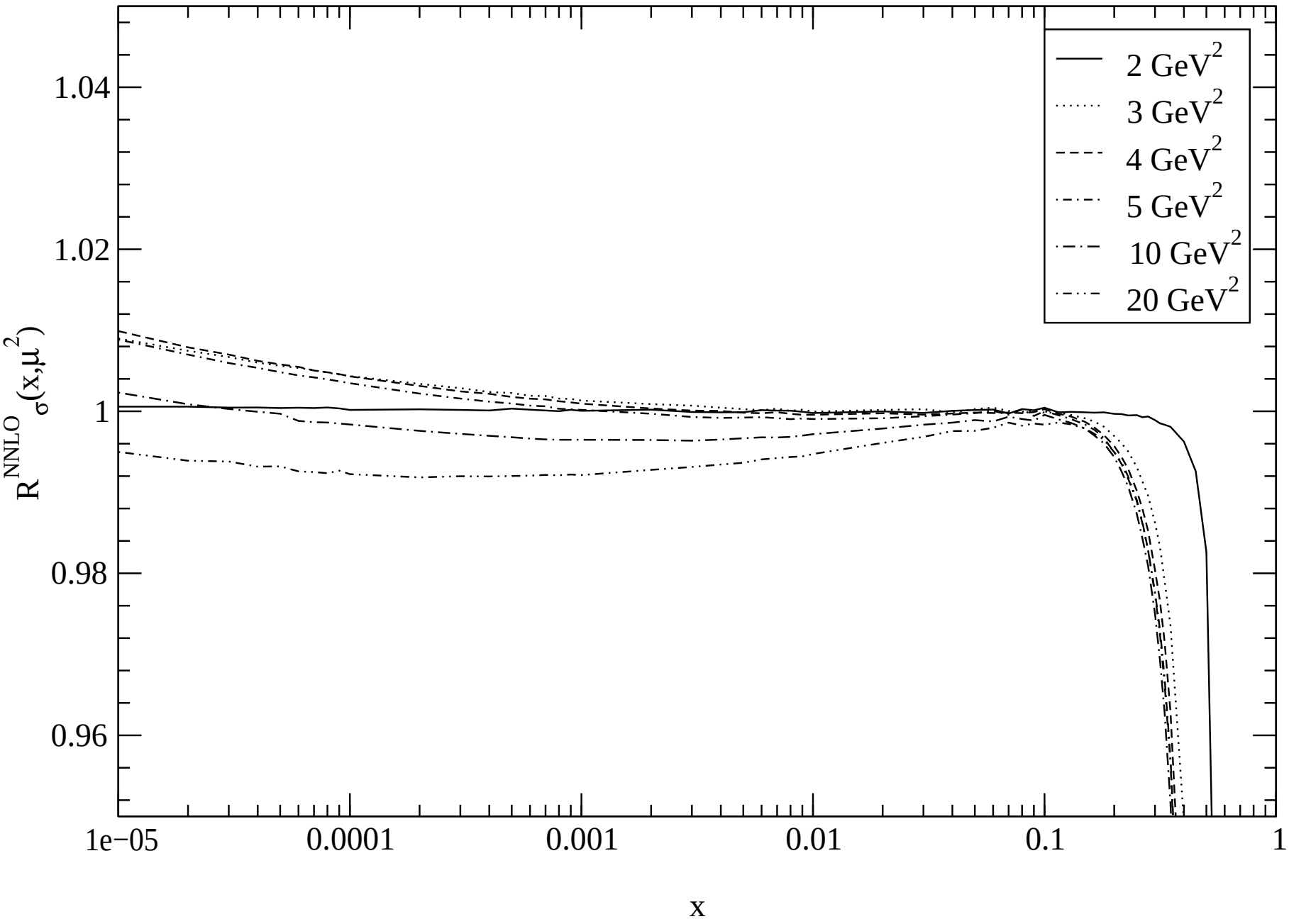
2 GeV^2
3 GeV^2
4 GeV^2
5 GeV^2
10 GeV^2
20 GeV^2
1.04
1.02
1
0.98
0.96
$R^{NNLO}_{\sigma}(x,\mu^2)$
1e−05
0.0001
0.001
0.01
0.1
1
x

Fig. 4(c)

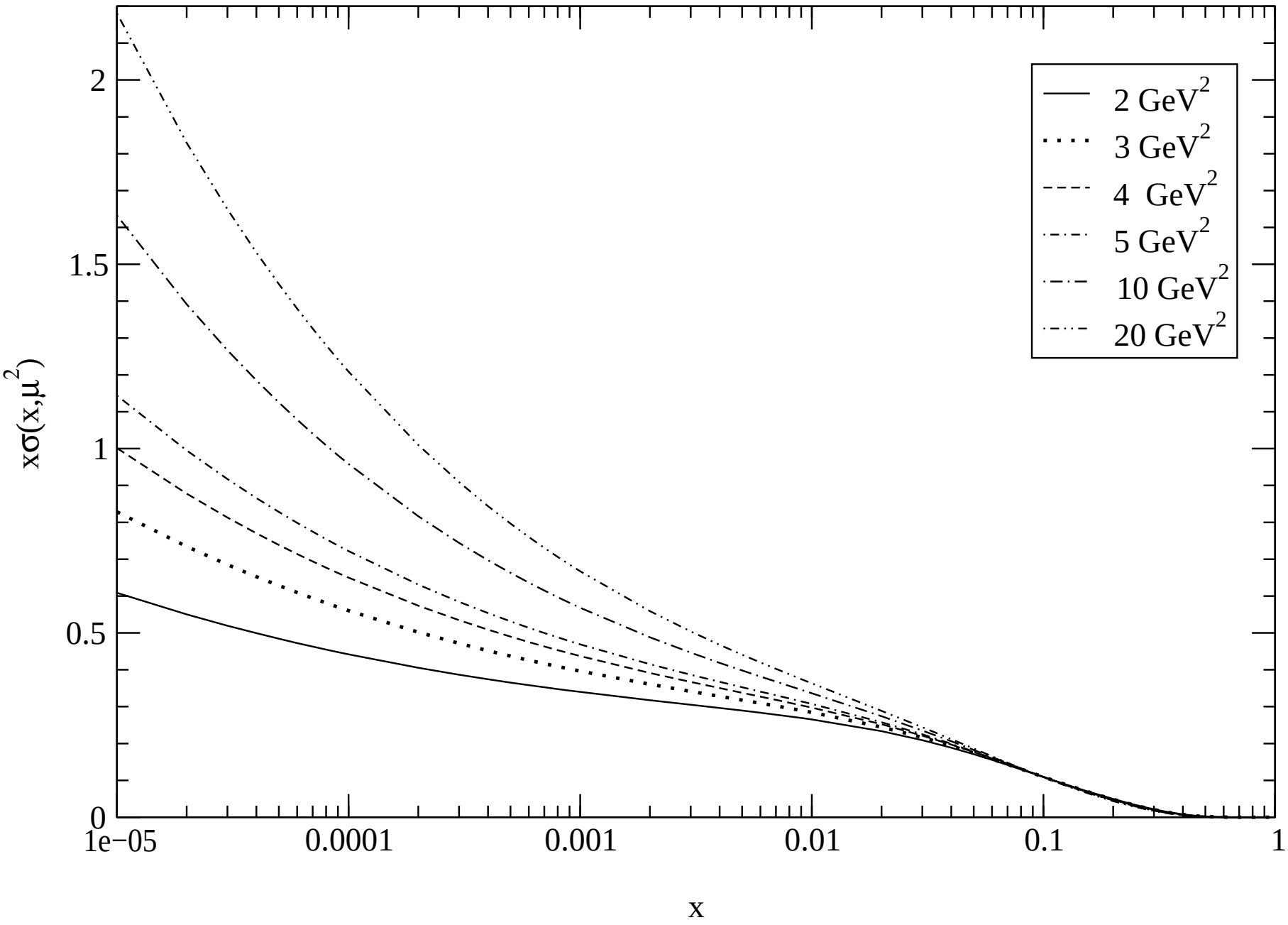
2 GeV^2
3 GeV^2
4 GeV^2
5 GeV^2
10 GeV^2
20 GeV^2
xσ(x,μ^2)
x
0
0.5
1
1.5
2
1e−05
0.0001
0.001
0.01
0.1
1

Fig. 5(a)

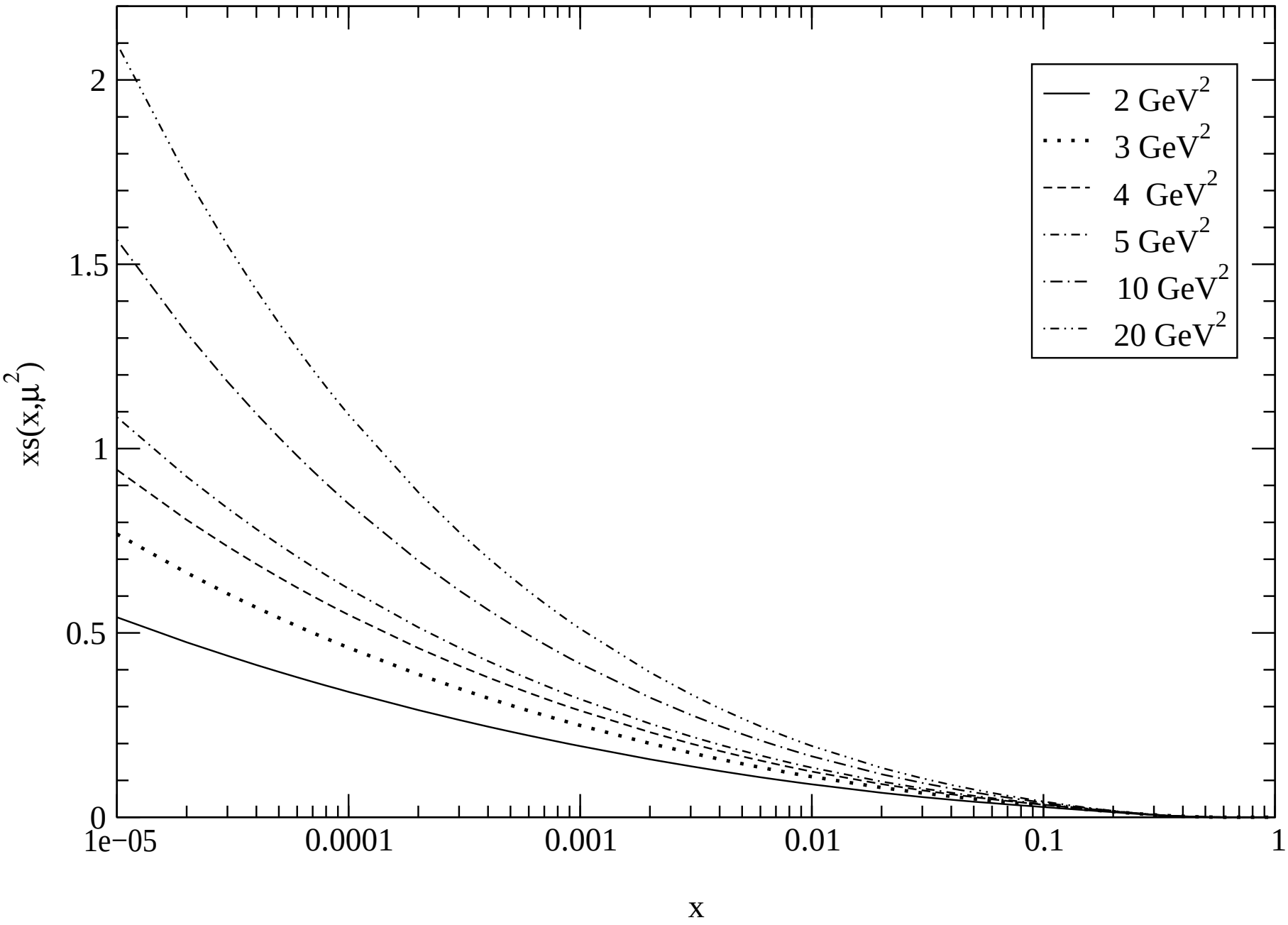
2 GeV^2
3 GeV^2
4 GeV^2
5 GeV^2
10 GeV^2
20 GeV^2
xs(x,μ^2)
x
0
0.5
1
1.5
2
1e−05
0.0001
0.001
0.01
0.1
1

Fig. 5(b)

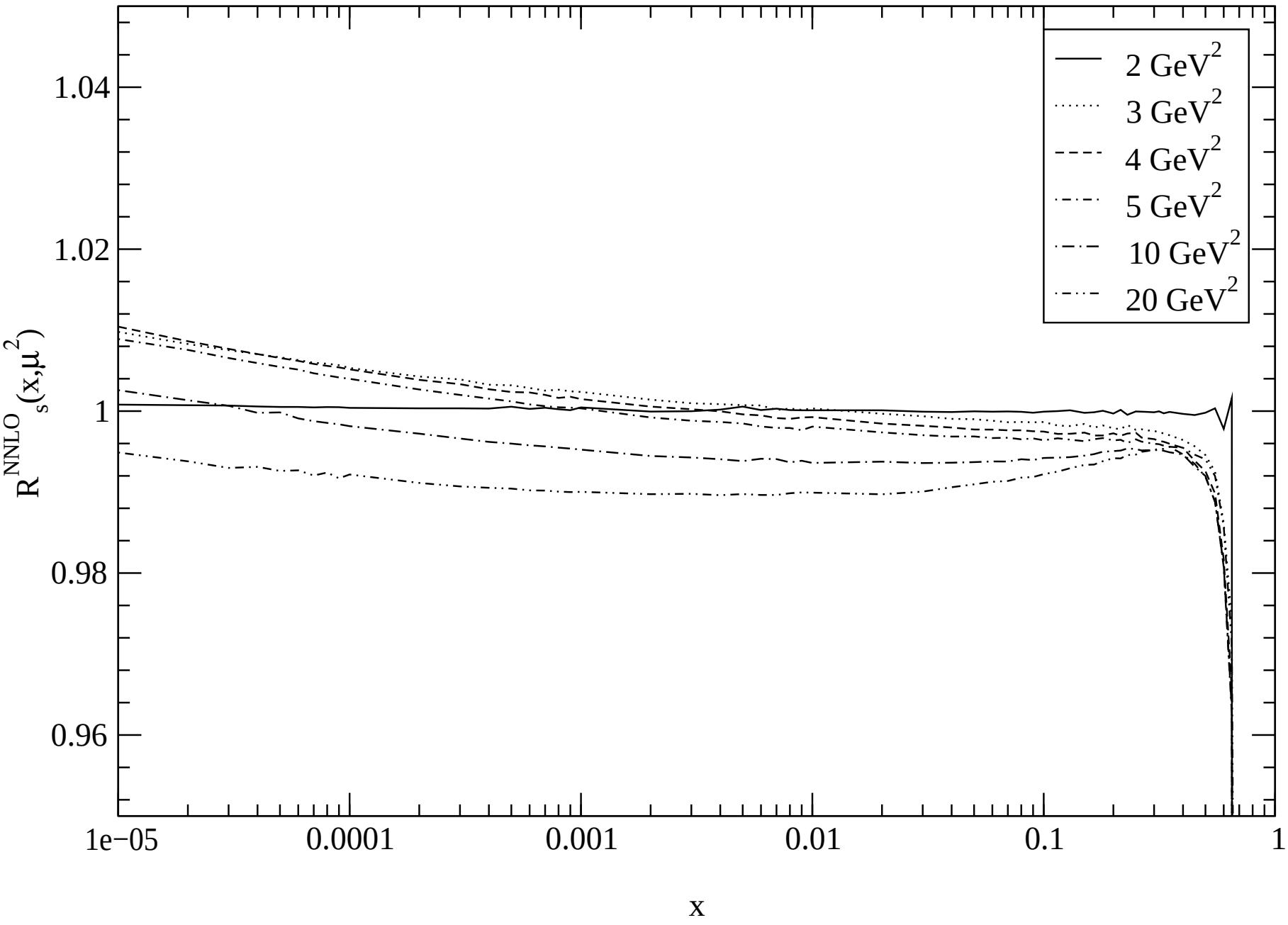
2 GeV^2
3 GeV^2
4 GeV^2
5 GeV^2
10 GeV^2
20 GeV^2
1.04
1.02
1
0.98
0.96
$R^{NNLO}_s(x,\mu^2)$
1e−05
0.0001
0.001
0.01
0.1
1
x

Fig. 5(c)

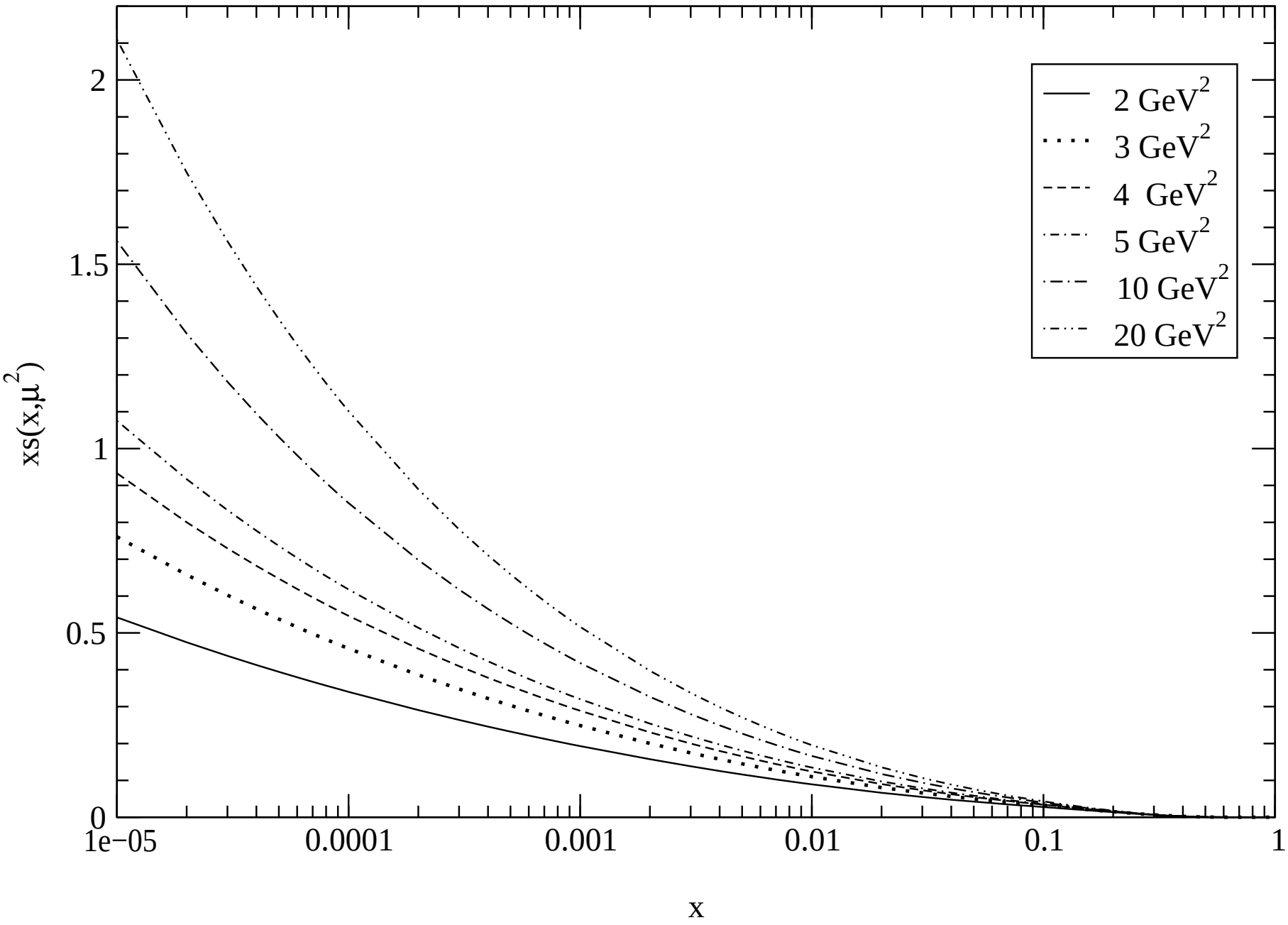
2 GeV^2
3 GeV^2
4 GeV^2
5 GeV^2
10 GeV^2
20 GeV^2
xs(x,μ^2)
x
0
0.5
1
1.5
2
1e−05
0.0001
0.001
0.01
0.1
1

Fig. 6(a)

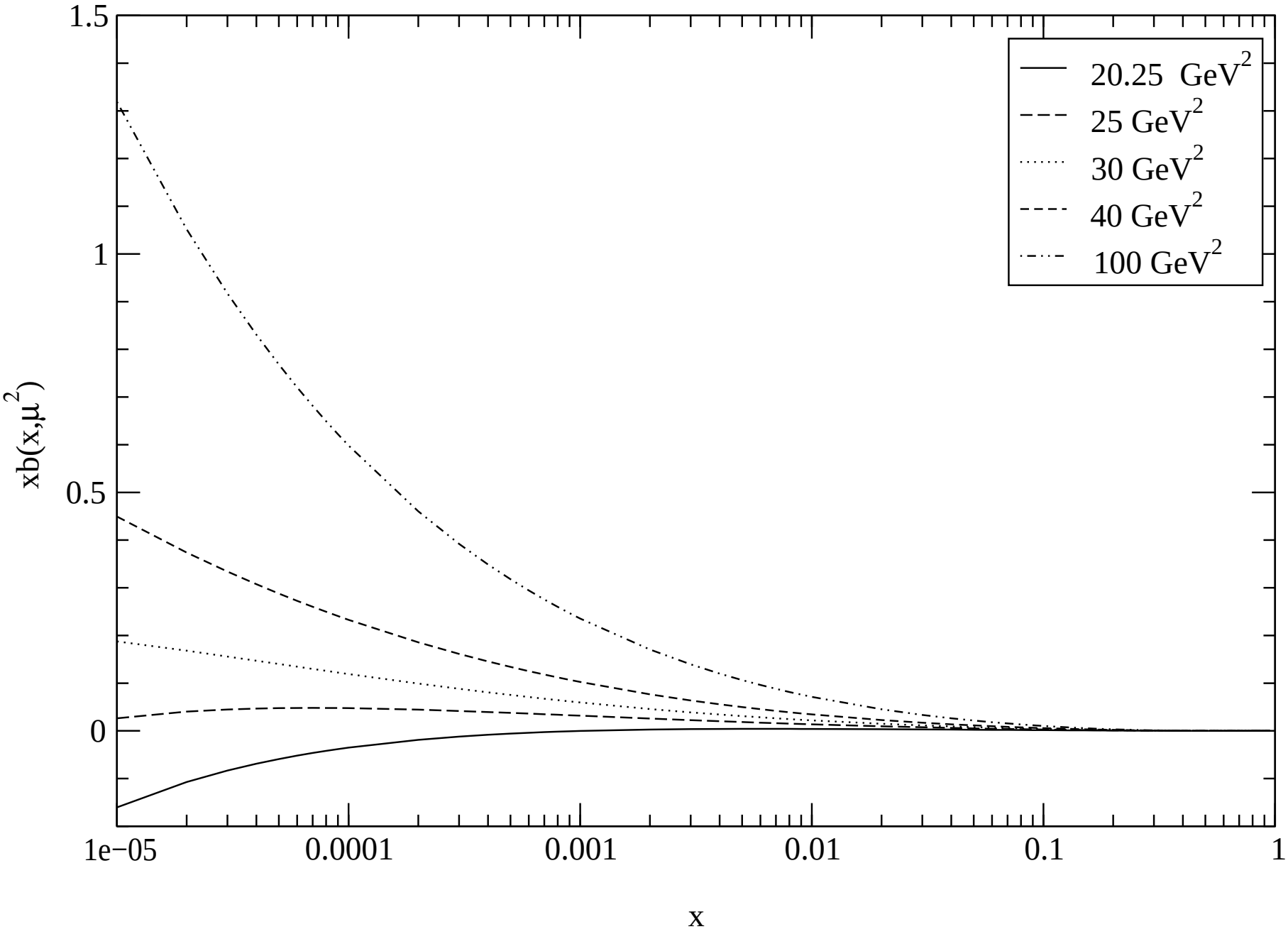
1.5
1
0.5
0
1e−05
0.0001
0.001
0.01
0.1
1
x
xb(x,μ2)
20.25 GeV2
25 GeV2
30 GeV2
40 GeV2
100 GeV2

Fig. 6(b)

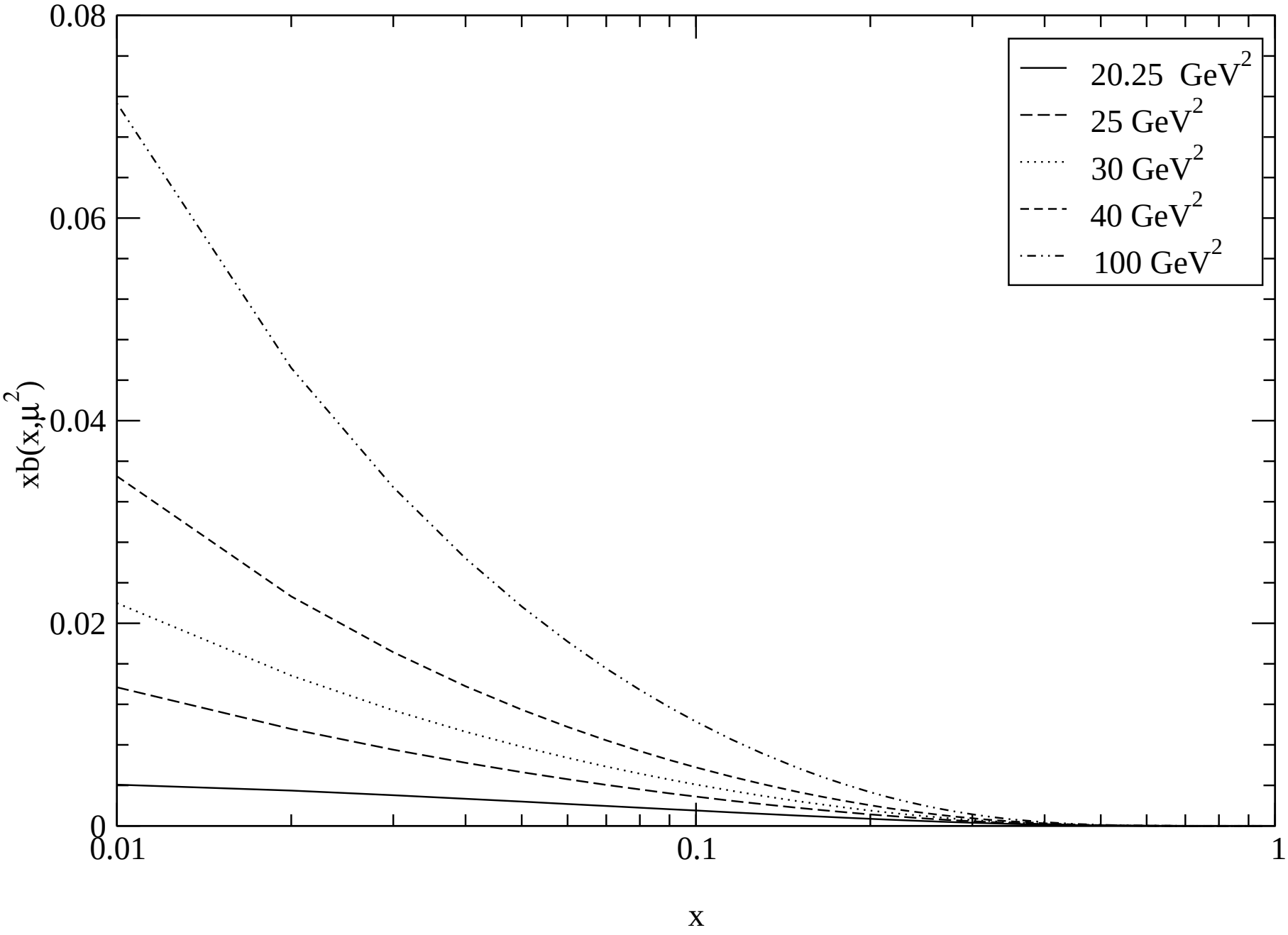
0.08
0.06
0.04
0.02
0
0.01
0.1
1
xb(x,μ^2)
x
20.25 GeV^2
25 GeV^2
30 GeV^2
40 GeV^2
100 GeV^2

Fig. 6(c)

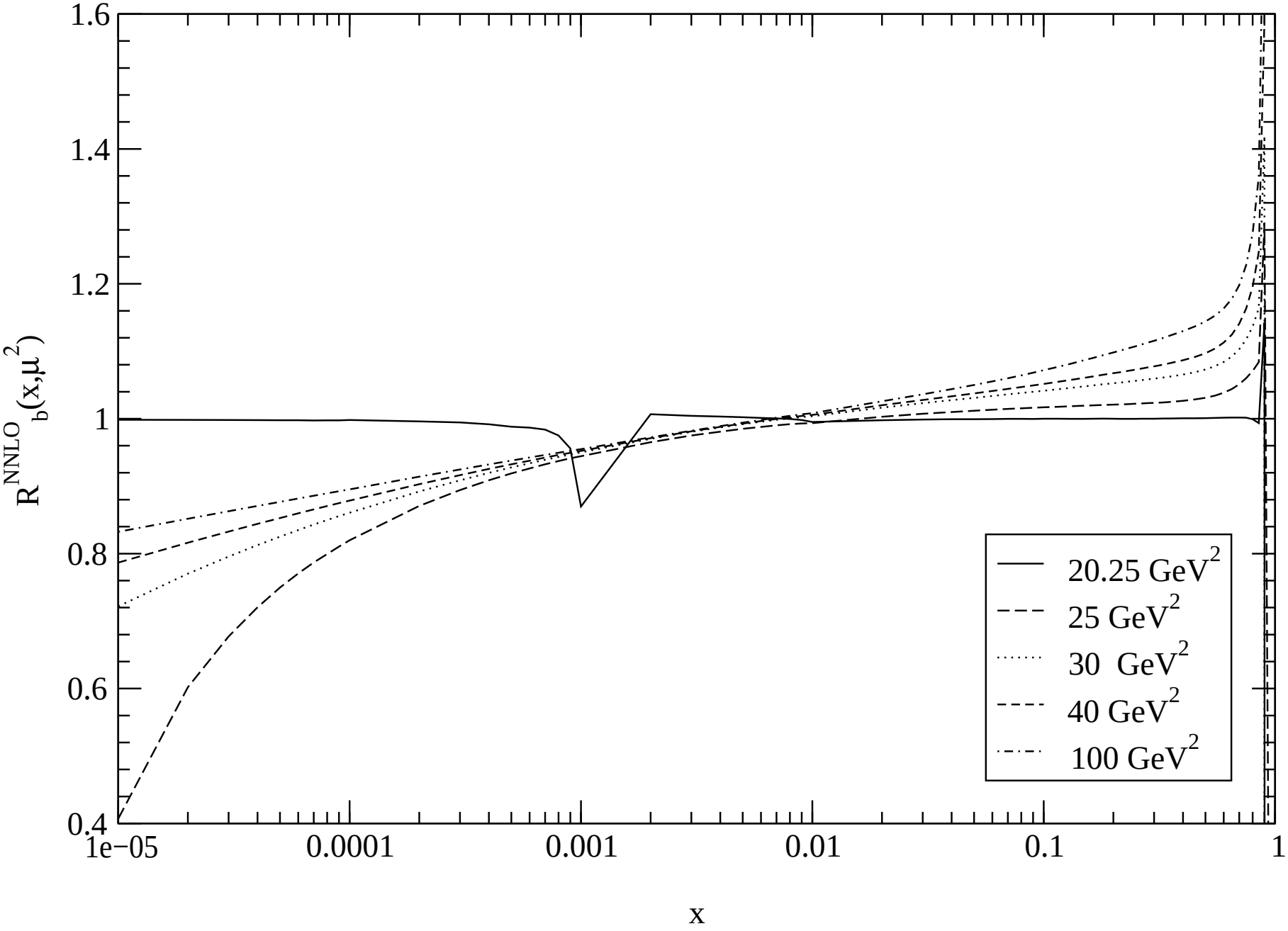
1.6
1.4
1.2
1
0.8
0.6
0.4
1e−05
0.0001
0.001
0.01
0.1
1
x
$R^{NNLO}_b(x,\mu^2)$
20.25 GeV^2
25 GeV^2
30 GeV^2
40 GeV^2
100 GeV^2

Fig. 6(d)

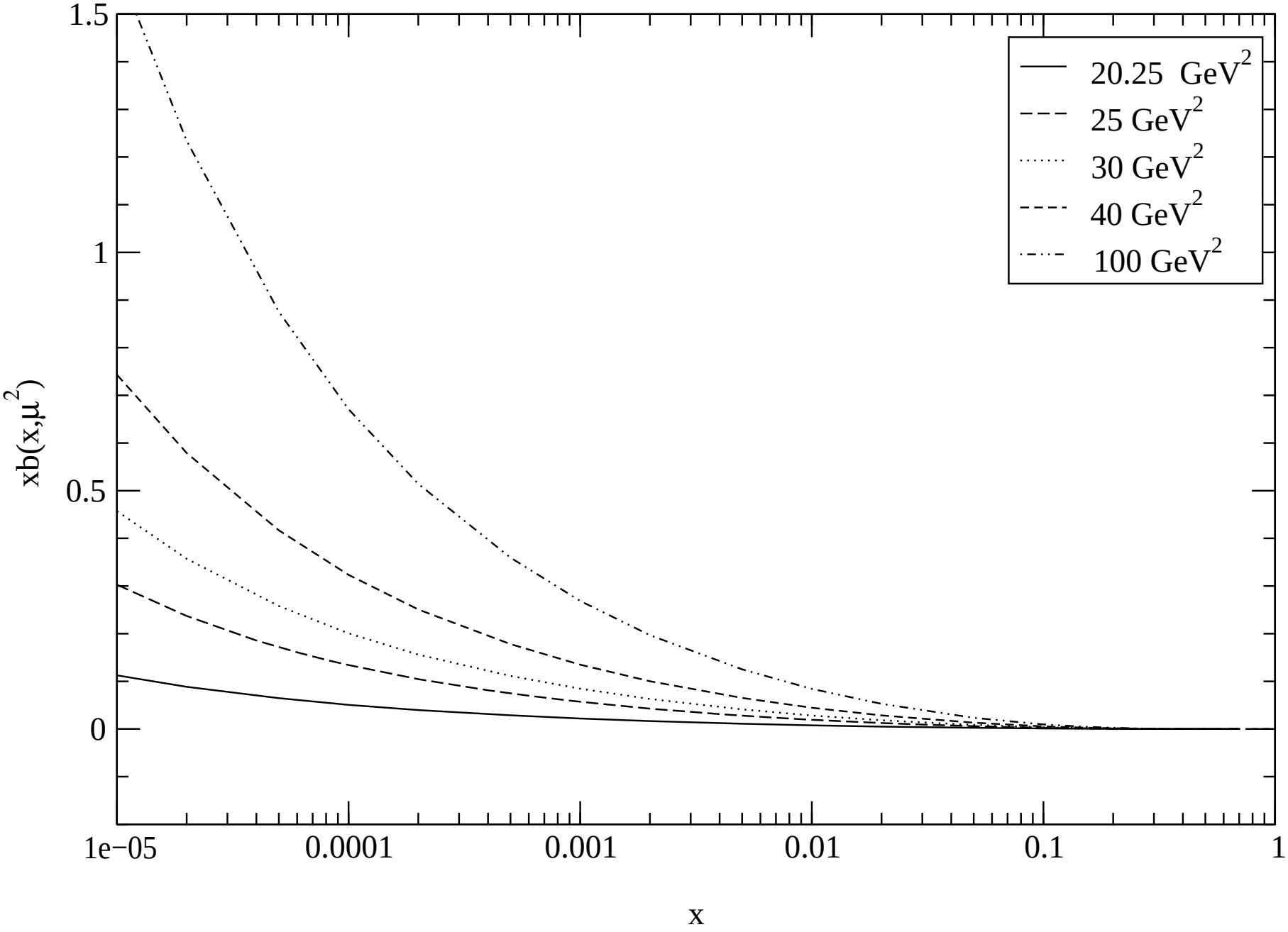
1.5
1
0.5
0
xb(x,μ^2)
1e−05
0.0001
0.001
0.01
0.1
1
x
20.25 GeV^2
25 GeV^2
30 GeV^2
40 GeV^2
100 GeV^2

Fig. 6(e)

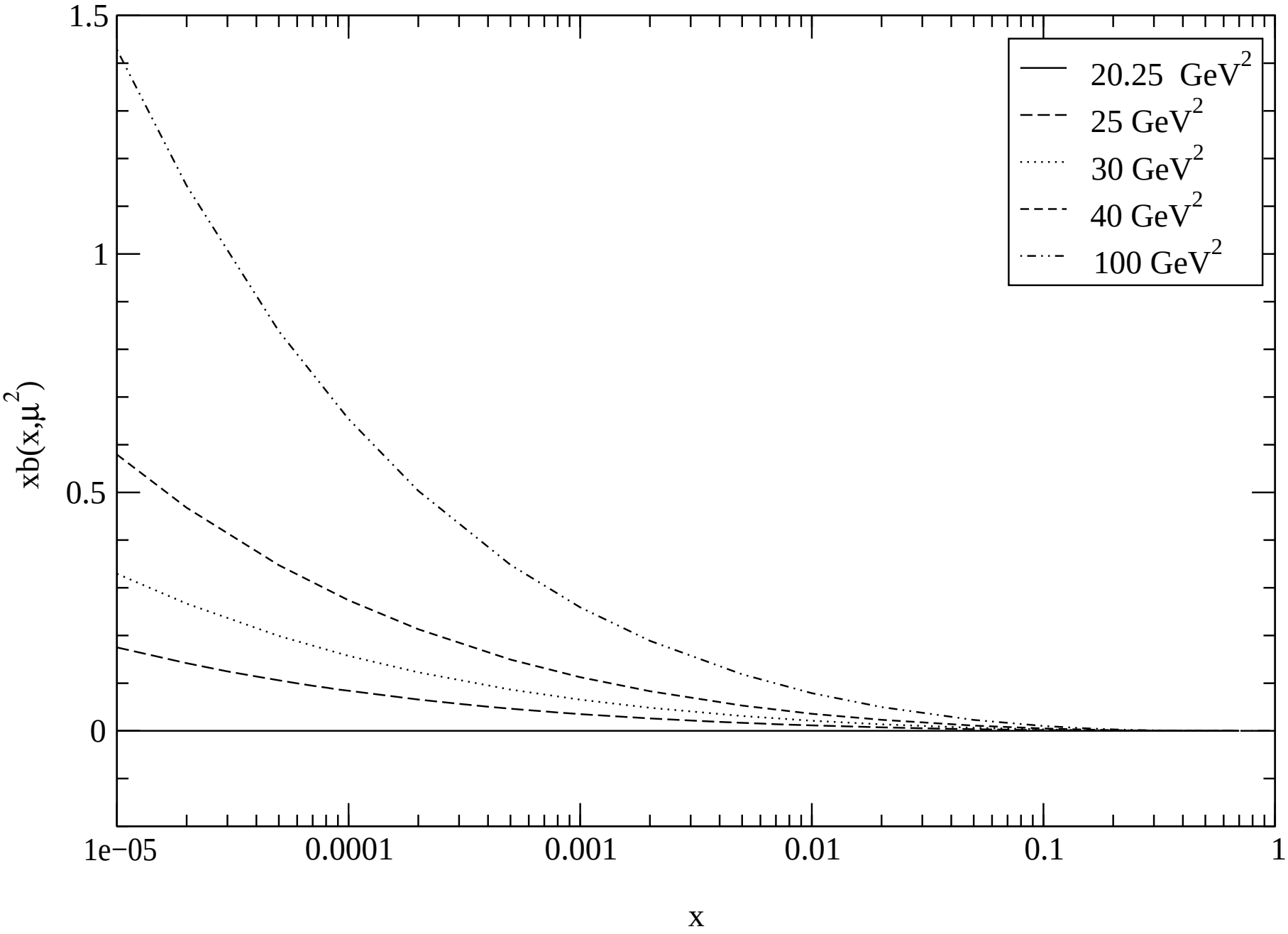
1.5
1
0.5
0
1e−05
0.0001
0.001
0.01
0.1
1
xb(x,μ2)
x
20.25 GeV2
25 GeV2
30 GeV2
40 GeV2
100 GeV2

Fig. 7(a)

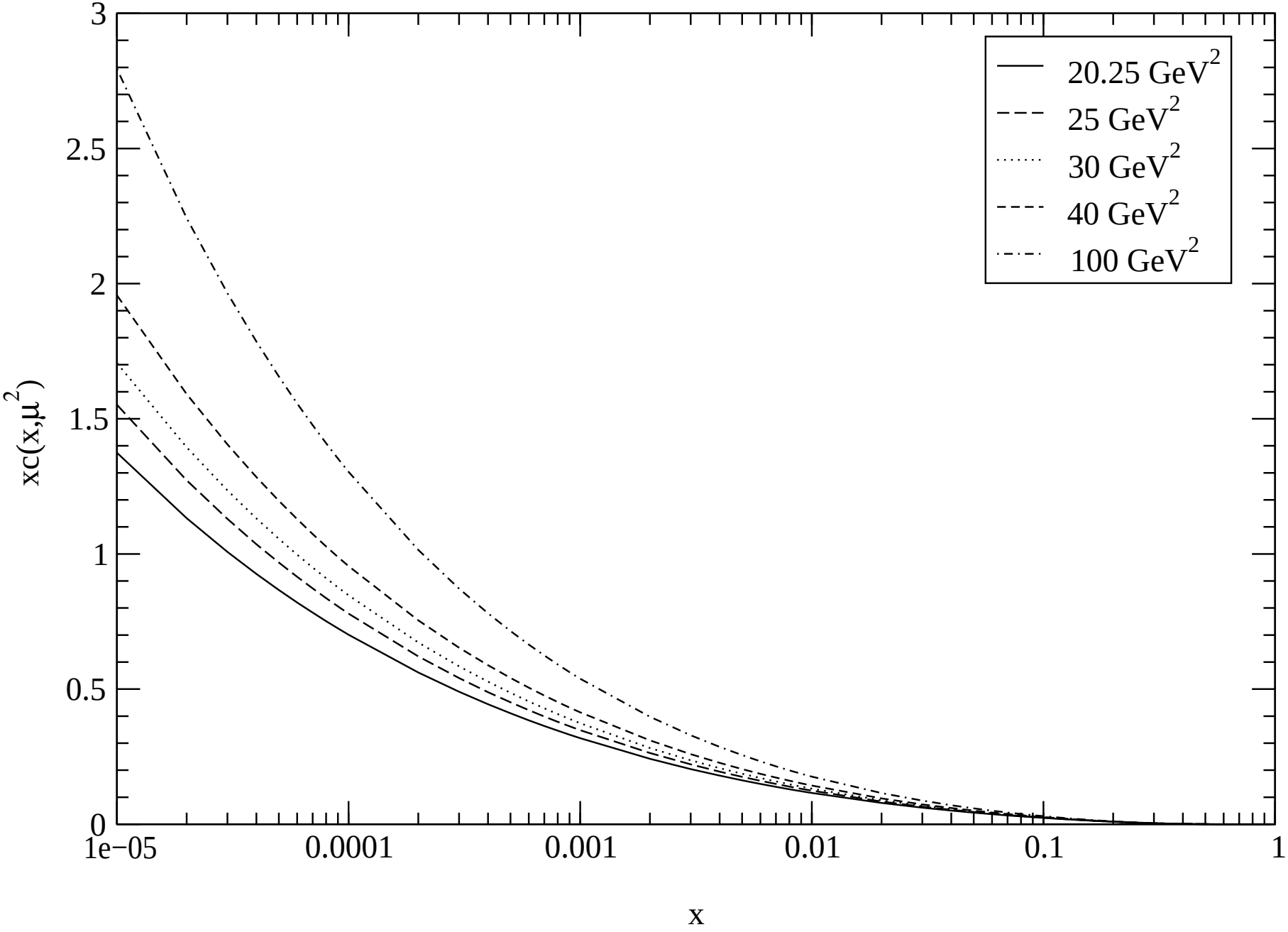
3
2.5
2
1.5
1
0.5
0
1e−05
0.0001
0.001
0.01
0.1
1
xc(x,μ2)
x
20.25 GeV2
25 GeV2
30 GeV2
40 GeV2
100 GeV2

Fig. 7(b)

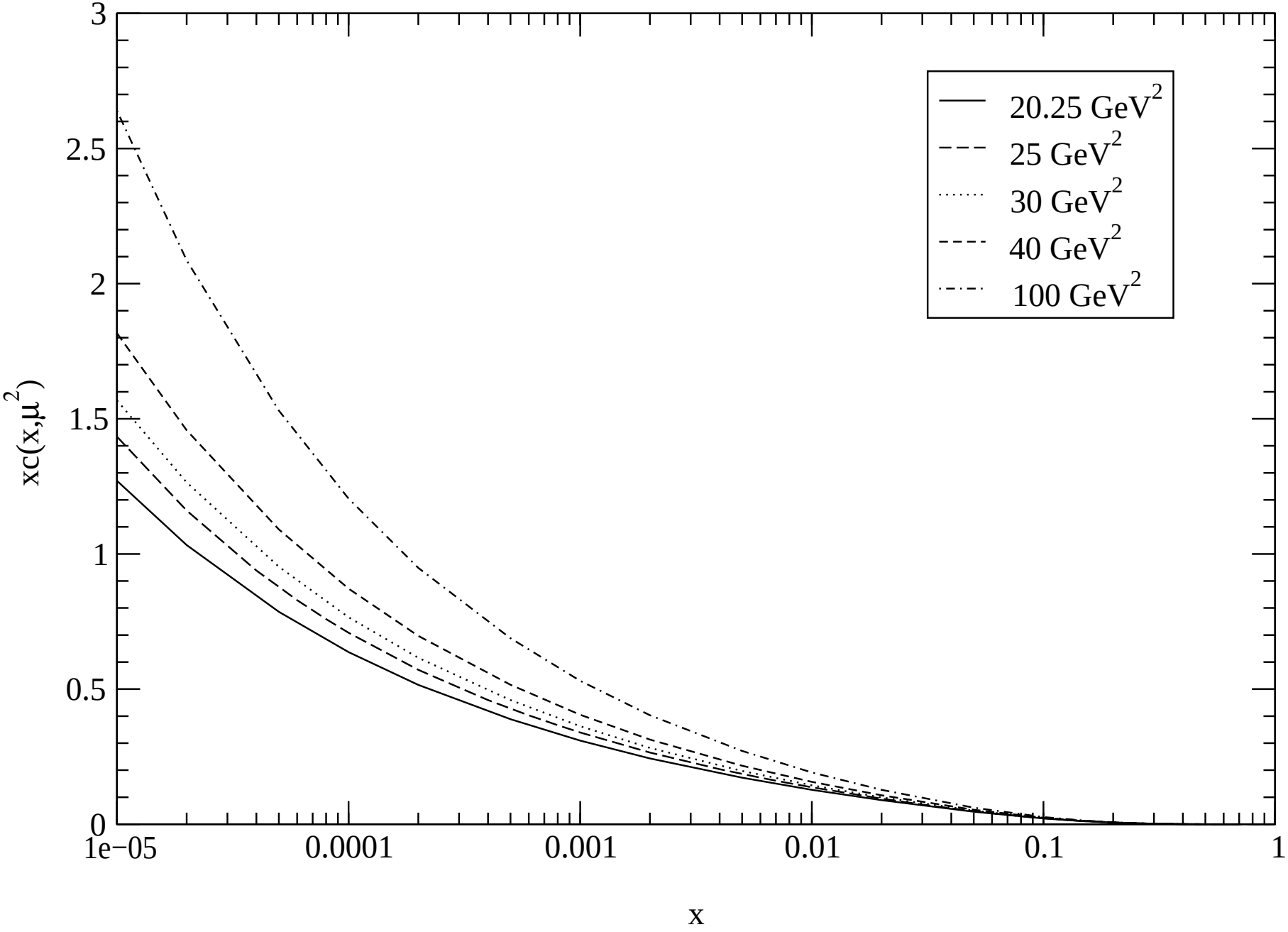
3
2.5
2
1.5
1
0.5
0
1e−05
0.0001
0.001
0.01
0.1
1
x
xc(x,μ2)
20.25 GeV2
25 GeV2
30 GeV2
40 GeV2
100 GeV2

Fig. 7(c)

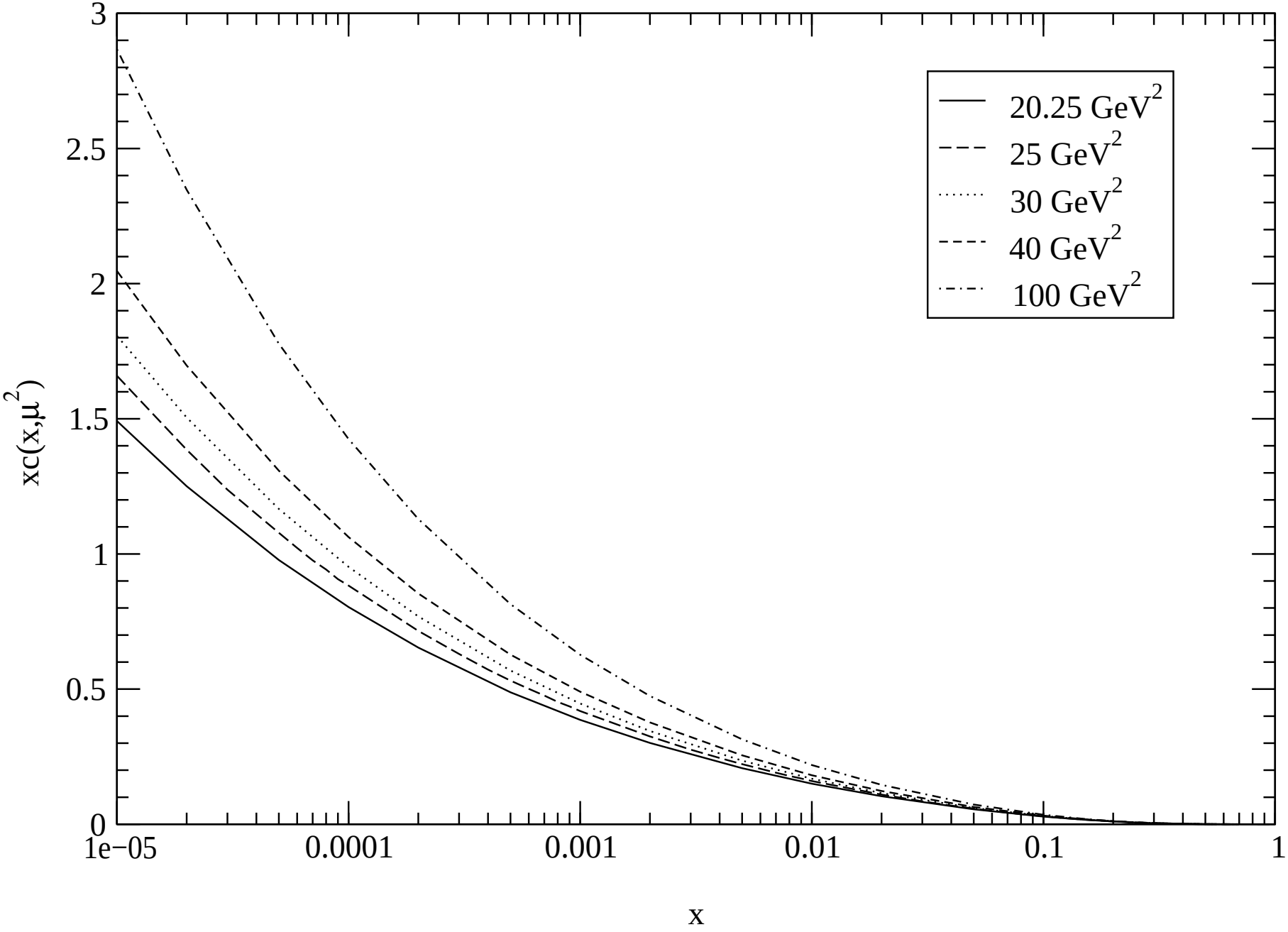
3
2.5
2
1.5
1
0.5
0
1e−05
0.0001
0.001
0.01
0.1
1
x
xc(x,μ2)
20.25 GeV2
25 GeV2
30 GeV2
40 GeV2
100 GeV2

Fig. 8(a)

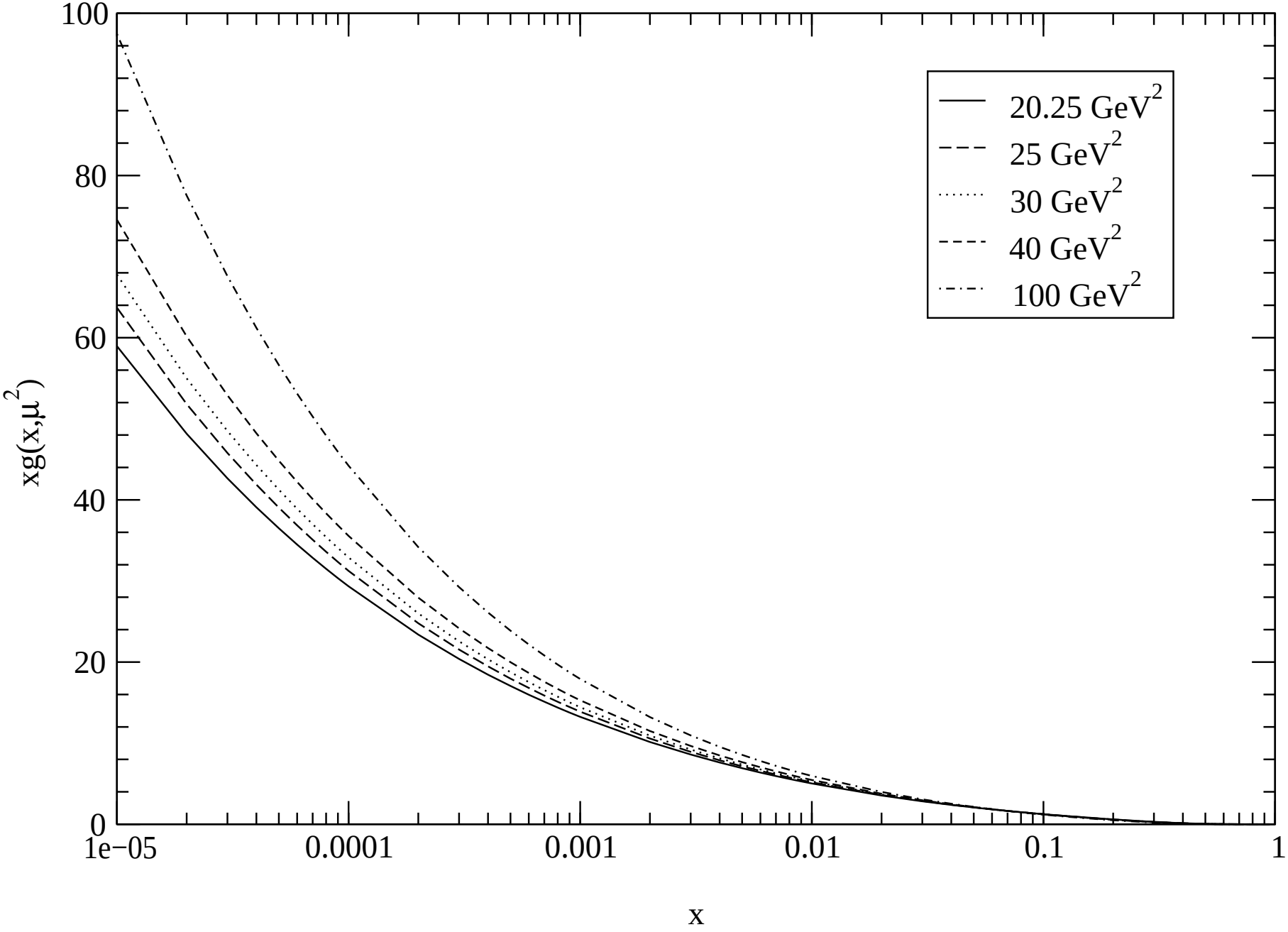
100
80
60
40
20
0
1e−05
0.0001
0.001
0.01
0.1
1
xg(x,μ2)
x
20.25 GeV2
25 GeV2
30 GeV2
40 GeV2
100 GeV2

Fig. 8(b)

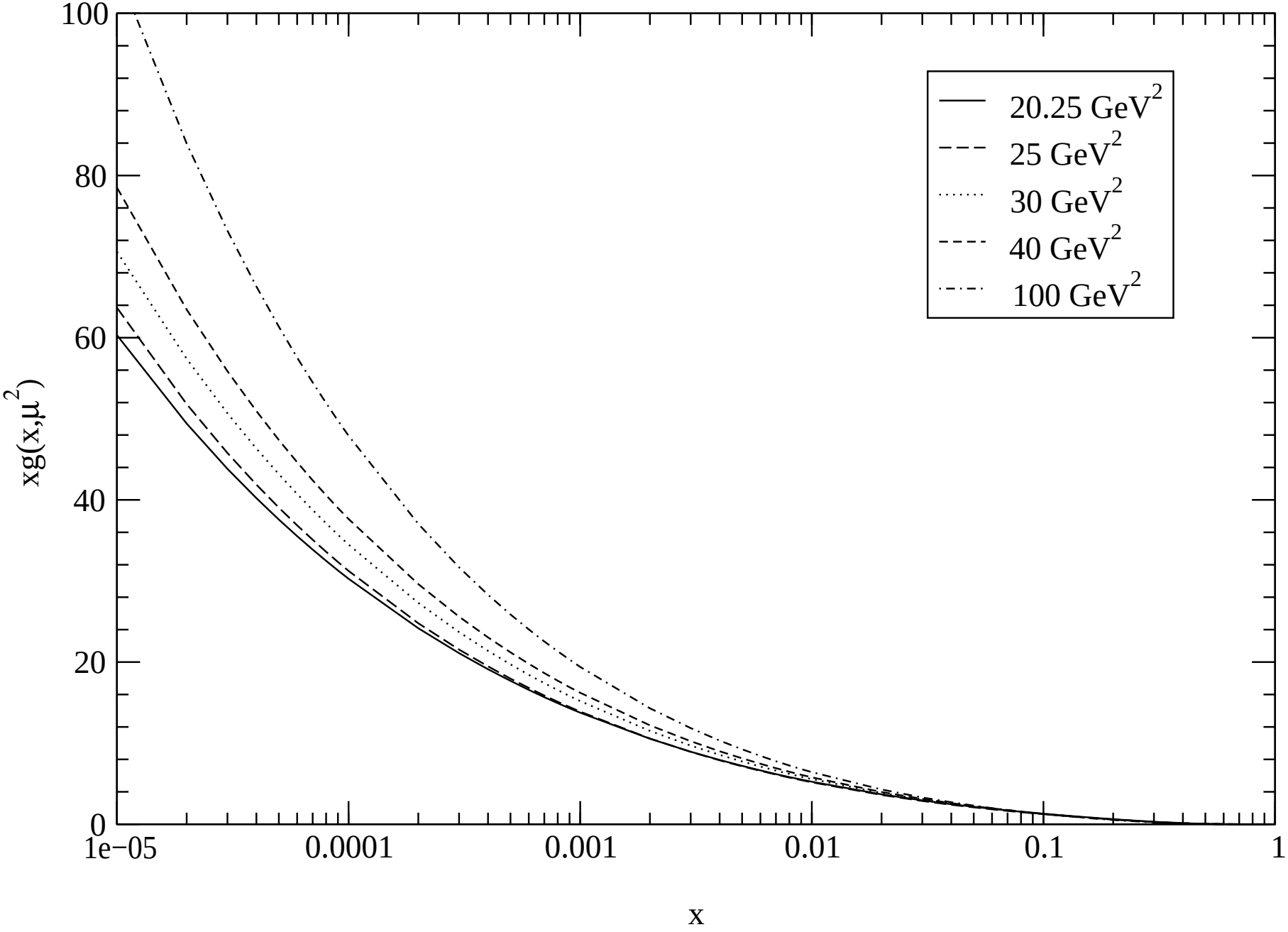
100
80
60
40
20
0
1e−05
0.0001
0.001
0.01
0.1
1
xg(x,μ2)
x
20.25 GeV2
25 GeV2
30 GeV2
40 GeV2
100 GeV2

Fig. 9(a)

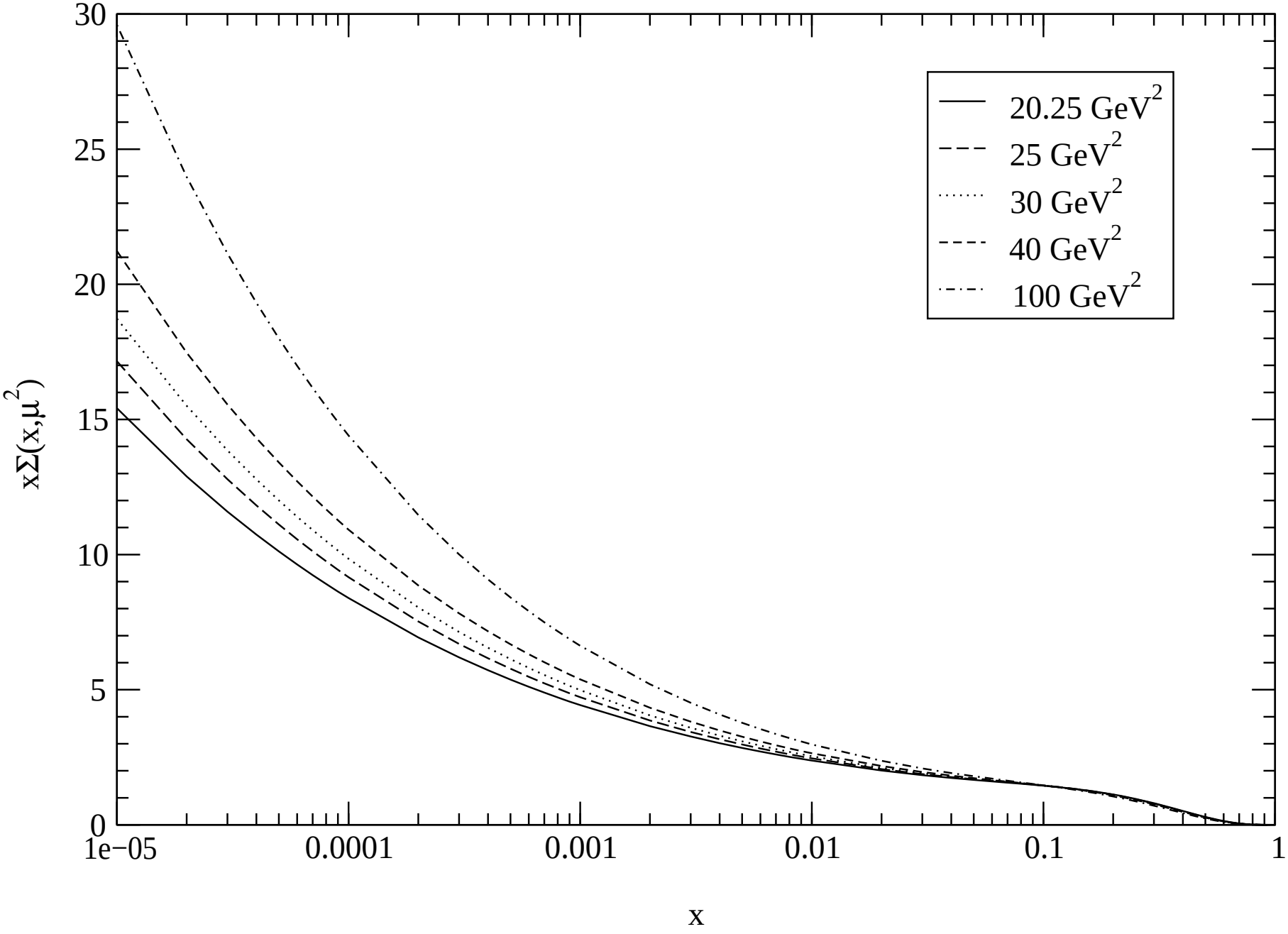
30
25
20
15
10
5
0
1e−05
0.0001
0.001
0.01
0.1
1
x
xΣ(x,μ2)
20.25 GeV2
25 GeV2
30 GeV2
40 GeV2
100 GeV2

Fig. 9(b)

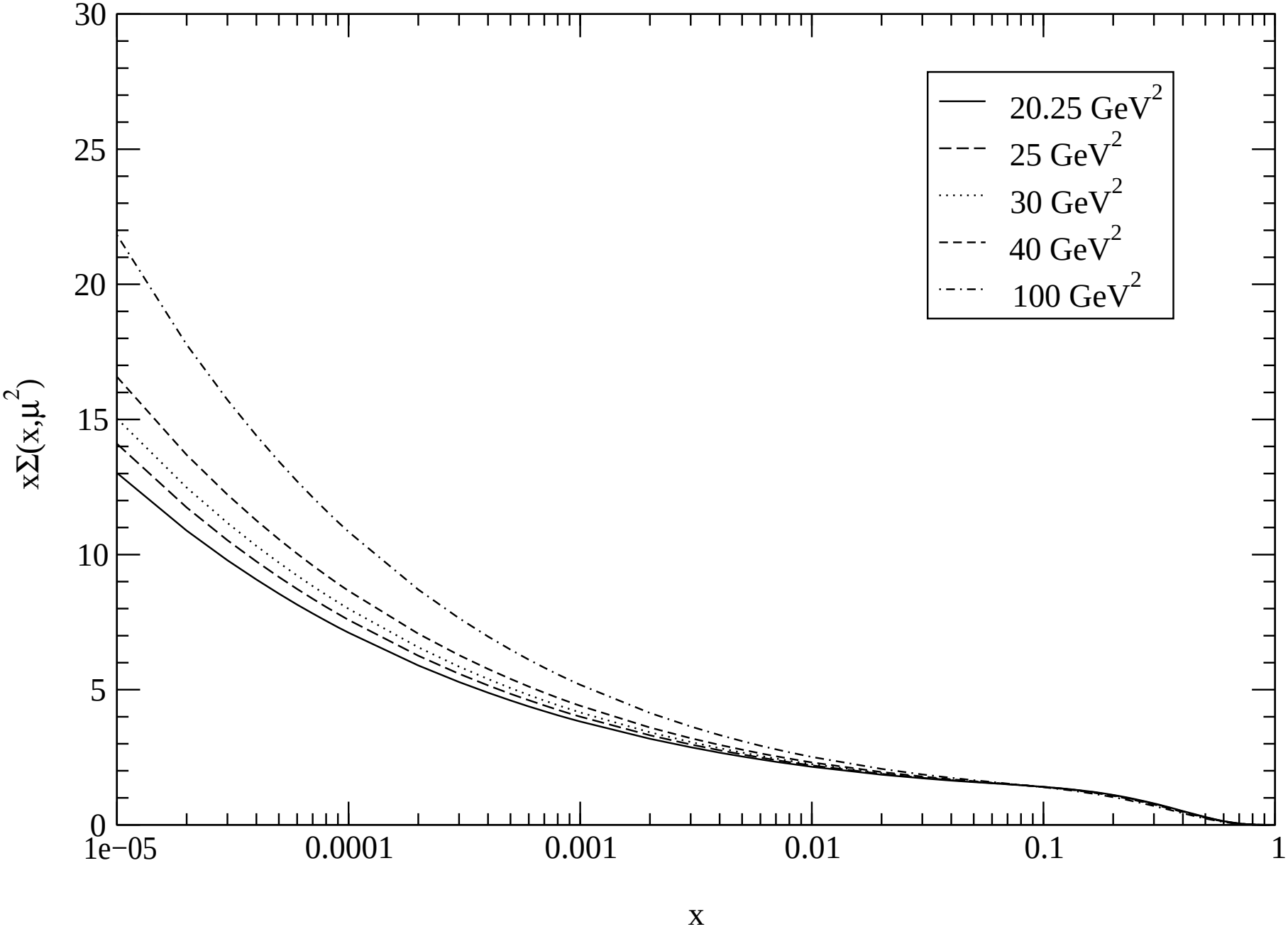
30
25
20
15
10
5
0
1e−05
0.0001
0.001
0.01
0.1
1
x
xΣ(x,μ2)
20.25 GeV2
25 GeV2
30 GeV2
40 GeV2
100 GeV2

Fig. 10(a)

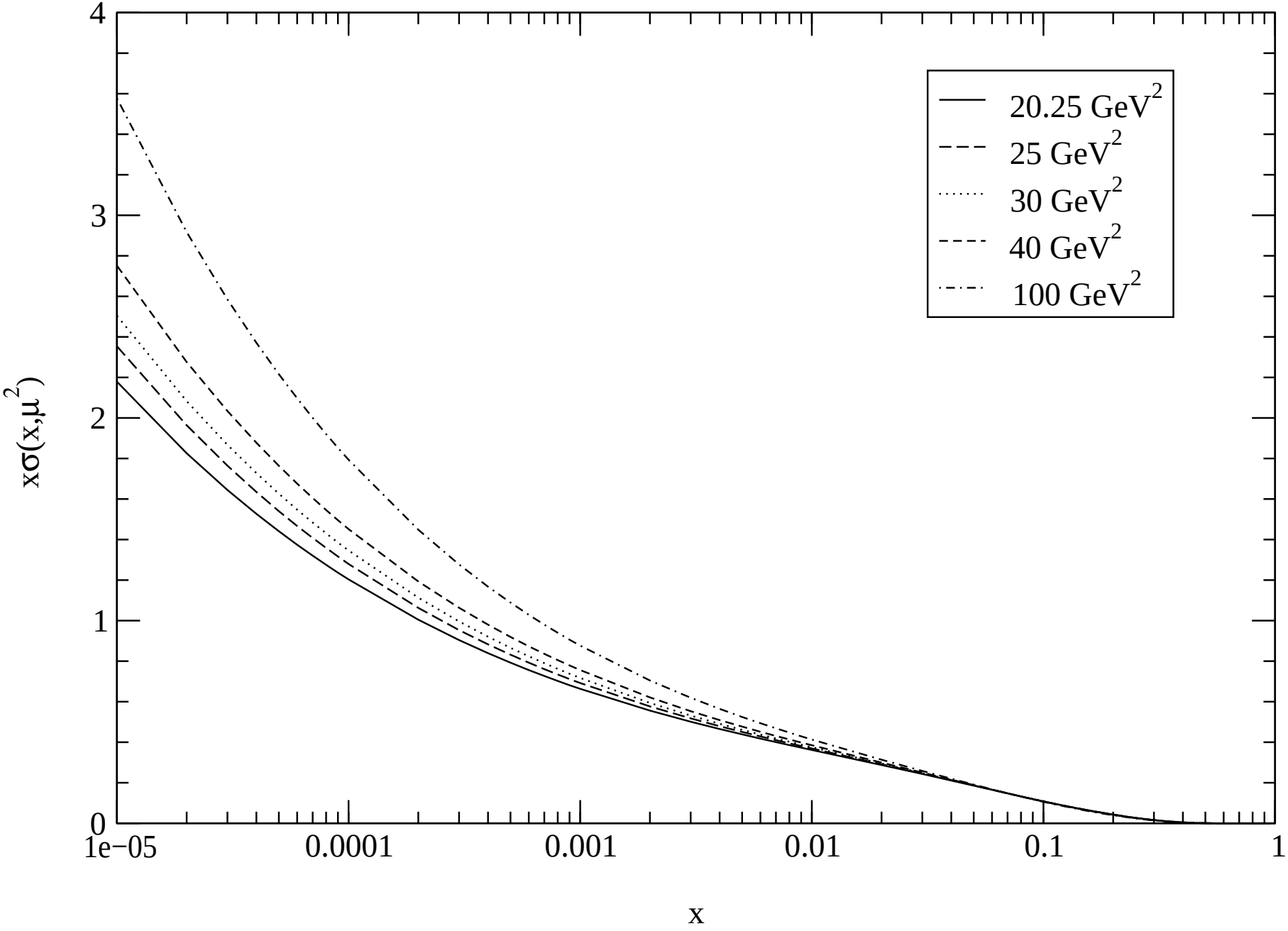
4
3
2
1
0
1e−05
0.0001
0.001
0.01
0.1
1
xσ(x,μ2)
x
20.25 GeV2
25 GeV2
30 GeV2
40 GeV2
100 GeV2

Fig. 10(b)

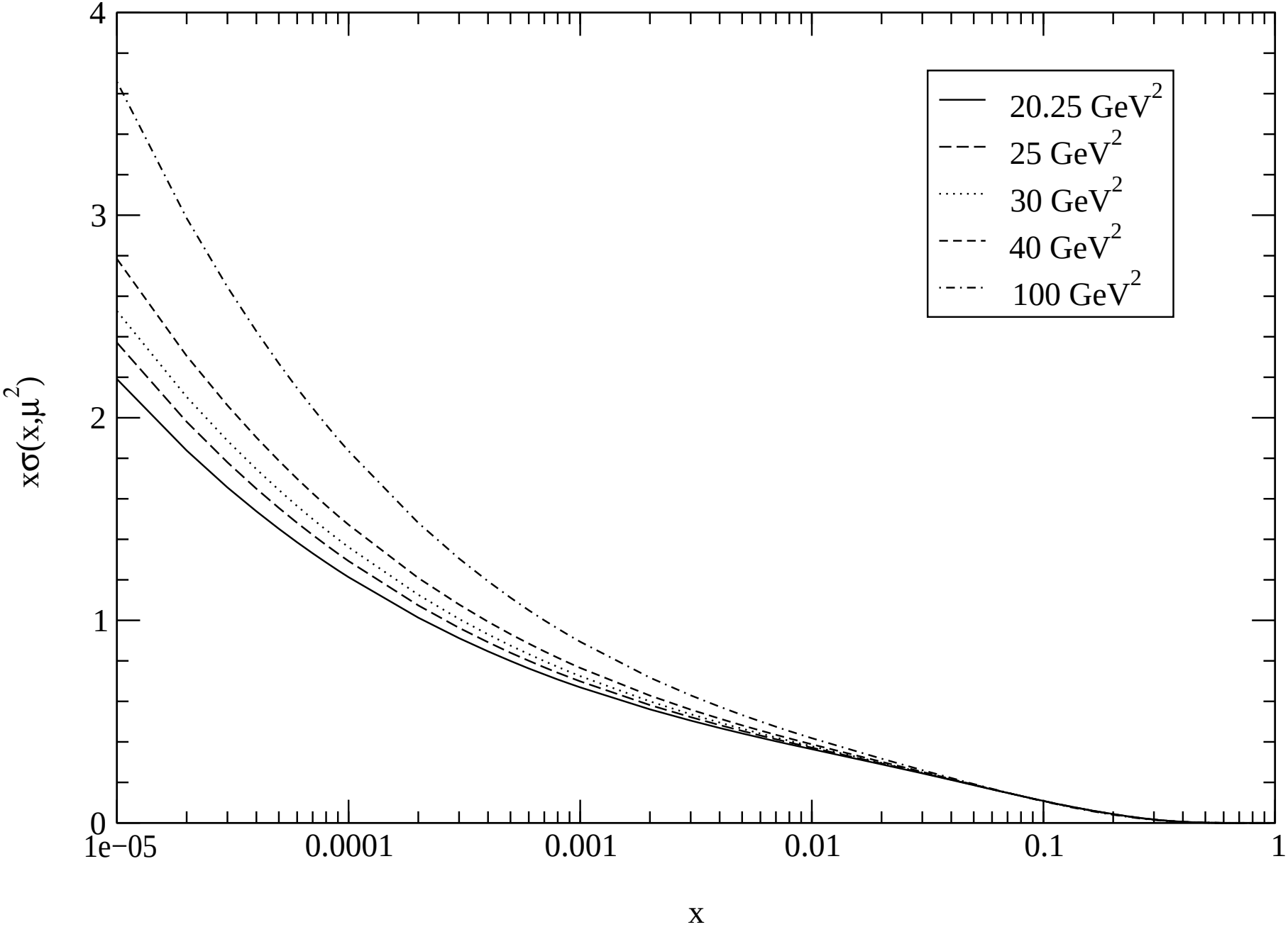
4
3
2
1
0
1e−05
0.0001
0.001
0.01
0.1
1
xσ(x,μ2)
x
20.25 GeV2
25 GeV2
30 GeV2
40 GeV2
100 GeV2

Fig. 11(a)

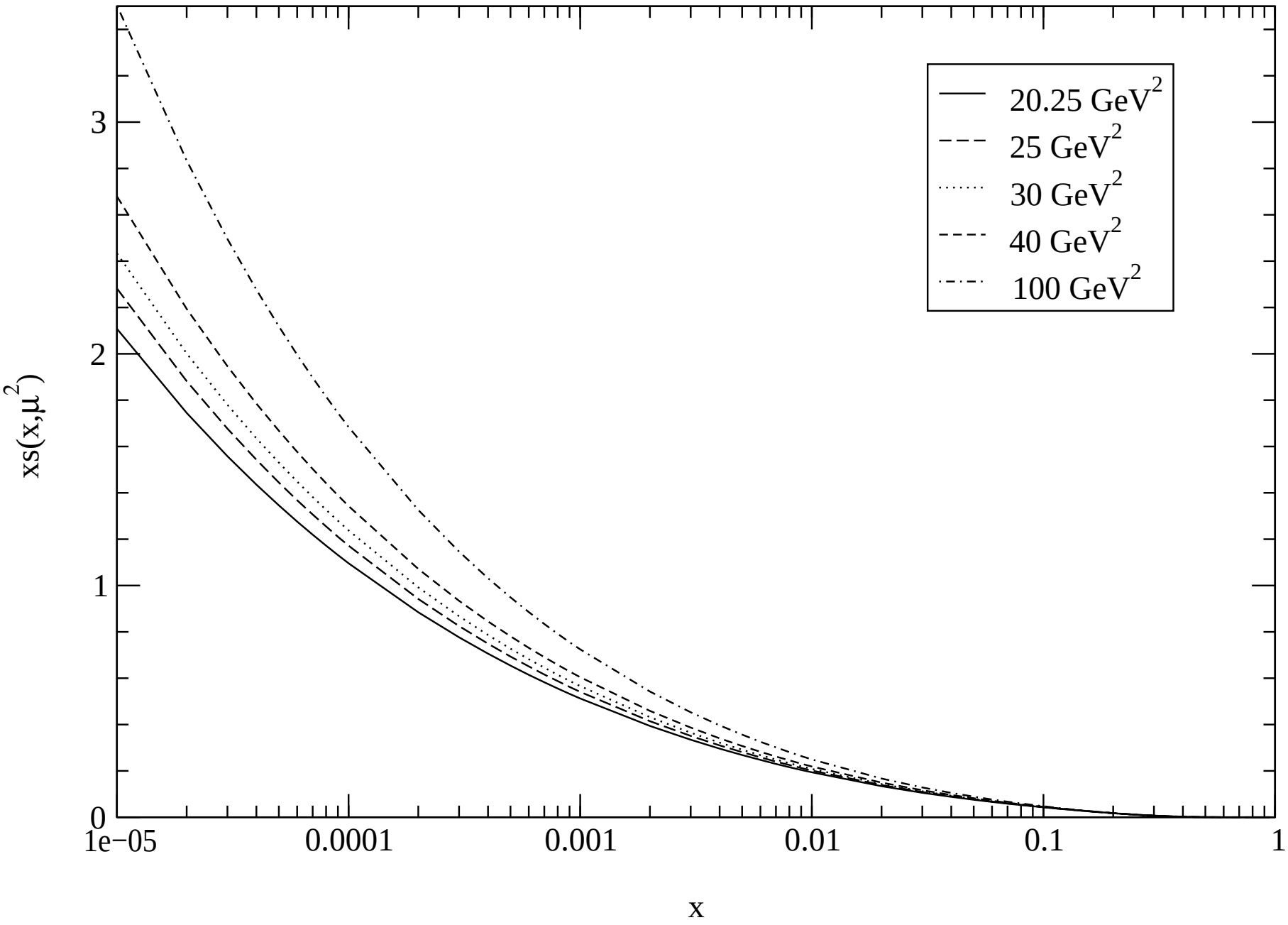
20.25 GeV^2
25 GeV^2
30 GeV^2
40 GeV^2
100 GeV^2
xs(x,μ^2)
x
0
1
2
3
1e−05
0.0001
0.001
0.01
0.1
1

Fig. 11(b)

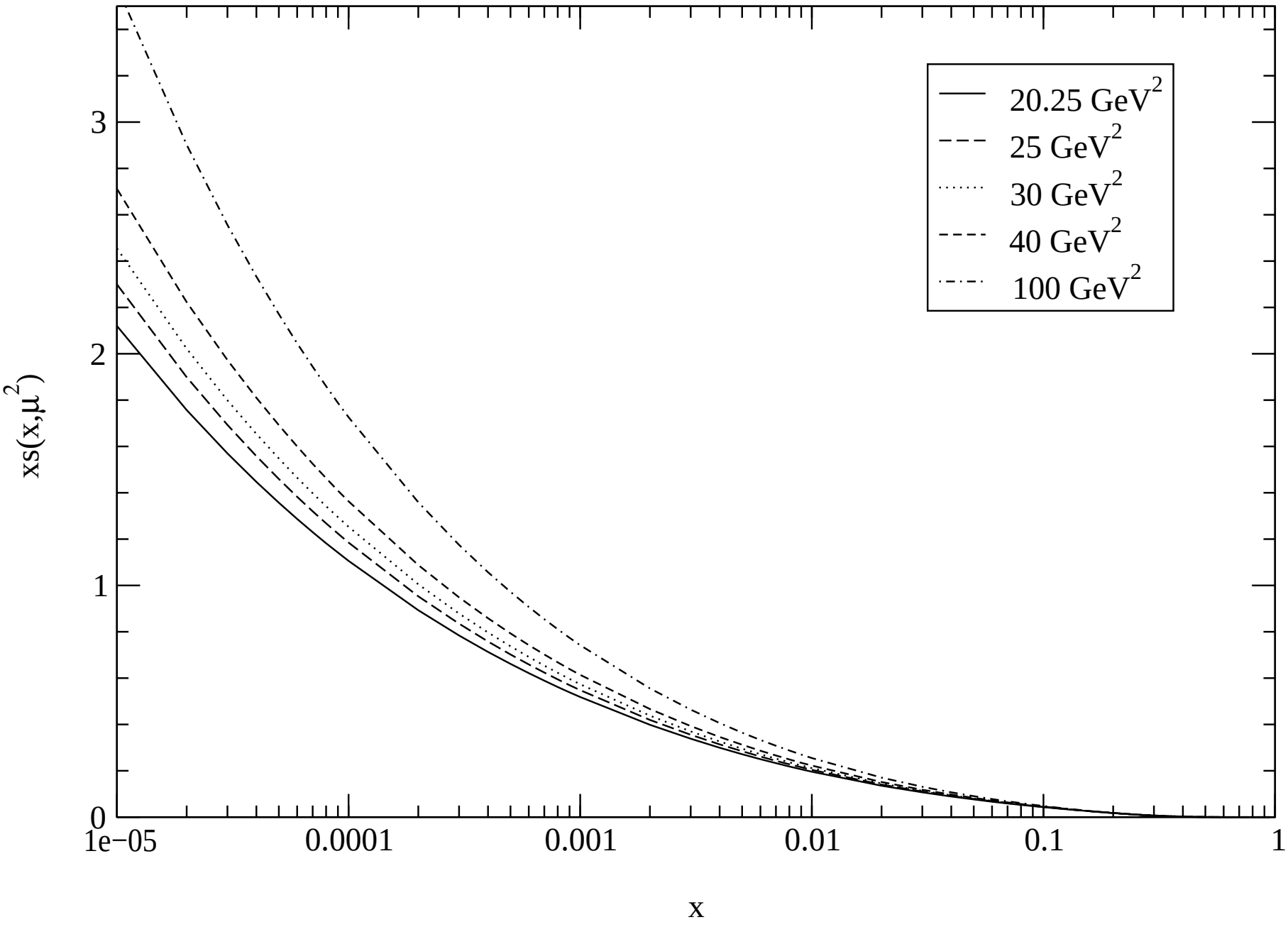
20.25 GeV^2
25 GeV^2
30 GeV^2
40 GeV^2
100 GeV^2
xs(x,μ^2)
x
0
1
2
3
1e−05
0.0001
0.001
0.01
0.1
1